University of Dundee

KEAP1-modifying small molecule reveals muted NRF2 signaling responses in neural stem cells from Huntington's disease patients

Quinti, Luisa; Dayalan Naidu, Sharadha; Träge, Ulrike ; Chen, Xiqun ; Kegel-Gleason, Kimberly ; Lleres, David; Connolly, Colúm ; Chopra, Vanita ; Low, Cho ; Moniot, Sebastien; Sapp, Ellen ; Tousley, Adelaide R; Vodicka, Petr ; Van Kanegan, Michael J.; Kaltenbach, Linda S.; Crawford, Lisa A; Fuszard, Matthew ; Higgins, Maureen; Miller, James R.C. ; Farmer, Ruth E. ; Potluri, Vijay ; Samajdar, Susanta ; Meisel, Lisa; Zhang, Ningzhe ; Snyder, Andrew ; Stein, Ross ; Hersch, Steven M. ; Ellerby, Lisa M.; Weerapana, Eranthie ; Schwarzschild, Michael A. ; Steegborn, Clemens; Leavitt, Blair R. ; Degterev, Alexei; Tabrizi, Sarah J. ; Lo, Donald C. ; DiFiglia, Marian ; Thompson, Leslie M.; Dinkova-Kostova, Albena; Kazantsev, Aleksey G.

BIOLOGICAL SCIENCES: Neuroscience

Title: A KEAP1-modifying small molecule reveals muted NRF2 signaling responses in neural stem cells from Huntington disease patients

Luisa Quinti[a,1], Sharadha Dayalan Naidu[b,1], Ulrike Träger[c,1], Xiqun Chen[a,1], Kimberly Kegel-Gleason[a], David Llères[d], Colúm Connolly[e], Vanita Chopra[a], Cho Low[f], Sébastien Moniot[g], Ellen Sapp[a], Adelaide R. Tousley[a], Petr Vodicka[a], Michael J. Van Kanegan[h], Linda S. Kaltenbach[h], Lisa A. Crawford[j], Matthew Fuszard[g], Maureen Higgins[b], James R.C. Miller[c], Ruth E. Farmer[k], Vijay Potluri[l], Susanta Samajdar[l], Lisa Meisel[g], Ningzhe Zhang[m], Andrew Snyder[n], Ross Stein[n], Steven M. Hersch[a], Lisa M. Ellerby[m], Eranthie Weerapana[j], Michael A. Schwarzschild[a], Clemens Steegborn[g], Blair R. Leavitt[e], Alexei Degterev[f], Sarah J. Tabrizi[c], Donald C. Lo[h], Marian DiFiglia[a], Leslie M. Thompson[o], Albena T. Dinkova-Kostova[b,p], and Aleksey G. Kazantsev[a,2]

Author's affiliation
a   Department of Neurology, Harvard Medical School and Massachusetts General
     Hospital, Boston, MA 02114
b   Division of Cancer Research, School of Medicine, University of Dundee, Dundee DD1
     9SY, Scotland, United Kingdom
c   Dept of Neurodegenerative Disease, Institute of Neurology, University College London,
     London, WC1N 3BG, United Kingdom
d   Institute of Molecular Genetics of Montpellier, Montpellier F-34293, France
e   Centre for Molecular Medicine and Therapeutics, Department of Medical
     Genetics, University of British Columbia, Vancouver, Canada V5Z 4H4
f   Department of Developmental, Molecular and Chemical Biology, Tufts University, Boston,
     MA 02111
g   Department of Biochemistry, University of Bayreuth, 95447, Bayreuth, Germany
h   Center for Drug Discovery and Department of Neurobiology, Duke University Medical
     Center, Durham, NC 27710
j   Department of Chemistry, Boston College, 2609 Beacon Street, Chestnut Hill, MA 02467
k   Department of Medical Statistics, London School of Hygiene and Tropical Medicine, London,
     WC1E 7HT, United Kingdom
l   Department of Medicinal Chemistry, Aurigene Discovery Technologies Limited 39-40,
     KIADB Industrial Area, Electronic City Phase II, Hosur Road, Bangalore-560 100, India
m   Buck Institute for Research on Aging, 8001 Redwood Blvd, Novato, CA 94945
n   Targanox, CBL, 1 Kendall Sq., Suite 2203 Bldg 200, Cambridge, MA 02139
o   Departments of Biological Chemistry, Neurobiology and Behavior, Psychiatry and Human
     Behavior University of California, Irvine, CA 92697
p   Departments of Medicine and Pharmacology and Molecular Sciences, Johns Hopkins
     University School of Medicine, Baltimore, MD 21205

Corresponding Author: Aleksey. G. Kazantsev, Department of Neurology, Harvard Medical School and Massachusetts General Hospital, Boston, MA 02114; Phone: 617-803-3702; Email: akazantsev47@gmail.com

[1] L.Q., S.D.N. and U.T. contribute equally to this work
[2] To whom correspondence may be addressed. Email: akazantsev47@gmail.com

Abstract

The activity of the transcription factor NRF2 (nuclear factor-erythroid 2 p45-derived factor 2) is orchestrated and amplified through enhanced transcription of antioxidant and anti-inflammatory target genes. The present study has characterized a thiazole-containing inducer of NRF2 and elucidated the mechanism by which this molecule activates NRF2 signaling. In a highly selective manner, the compound covalently modifies a critical stress-sensor cysteine (C151) of the E3 ligase substrate adaptor protein KEAP1 (Kelch-like ECH associated protein 1), the primary negative regulator of NRF2. We further used this inducer to probe the functional consequences of selective activation of NRF2 signaling in Huntington's disease (HD) mouse and human model systems. Surprisingly, we discovered a muted NRF2 activation response in human HD neural stem cells, which was restored by genetic correction of the disease-causing mutation. In contrast, selective activation of NRF2 signaling potently repressed the release of the pro-inflammatory cytokine IL-6 in primary mouse HD and wild-type microglia and astrocytes. Moreover, in primary monocytes from HD patients and healthy subjects, NRF2 induction repressed expression of the pro-inflammatory cytokines IL-1, IL-6, IL-8, and TNFα. Together, our results demonstrate a multifaceted protective potential of NRF2 signaling in key cell types relevant to HD pathology.

Significance Statement

Chronic neuroinflammation and oxidative stress are likely complicit in driving disease progression in Huntington's disease (HD). Here, the mechanism of action of a novel chemical scaffold is described that is highly selective for activation of NRF2, the master transcriptional regulator of cellular anti-inflammatory and antioxidant defense genes. The use of this scaffold revealed that NRF2-activation responses were muted in HD patient-derived neural stem cells, suggesting increased susceptibility of this critical renewable cell population to oxidative stress in HD brain. However, pharmacological activation of NRF2 was able to repress inflammatory responses in mouse microglia and astrocytes, the principal cellular mediators of neuroinflammation, and in blood monocytes from HD patients. Our results suggest multiple protective benefits of NRF2 activation for HD patients.

Introduction

NRF2 (NF-E2 p45-related factor 2)-mediated signaling is a major endogenous cellular defense mechanism against oxidative and xenobiotic stress (1-3). The transcription factor NRF2 is tightly regulated in the cytoplasm by KEAP1 (Kelch-like ECH associated protein 1), acting as an adaptor between NRF2 and CUL3-based E3 ubiquitin ligase (1, 4-6). In the absence of stress, KEAP1 efficiently mediates the polyubiquitination of NRF2 leading to its degradation by the UPS (ubiquitin-proteasome degradation system) (7-10). During stress conditions, oxidants or electrophiles chemically modify KEAP1 sensor cysteines, causing a conformational change of the protein KEAP1/NRF2/CUL3 complex, and impair NRF2 degradation (11-14). *De novo* synthesized NRF2 accumulates to levels overcoming the endogenous sequestration capacity of the remaining free KEAP1, at which point excess NRF2 translocates to the nucleus, binds to antioxidant response elements (AREs) in the promoter/enhancer regions of target genes, and broadly activates transcriptional responses (2, 12, 15). In this manner, NRF2 coordinates the transcriptional regulation of genes encoding phase II enzymes: NQO1 (NAD(P)H: quinone oxidoreductase 1); HO-1 (heme oxygenase (decycling) 1); catalytic (GCLC) and regulatory (GCLM) subunits of glutamate-cysteine ligase, and ~100 additional downstream targets (2, 16). Additional robust anti-inflammatory effects occur through NRF2 activation through molecular mechanisms that are just emerging (17). Nevertheless, there is already a strong body of empirical evidence *in vitro* and *in vivo* linking NRF2 activation and suppression of inflammation (18-20).

Oxidative stress and neuroinflammation are among the common pathogenic mechanisms implicated in neurodegenerative disorders, including Huntington's disease (HD) (21, 22). HD, an autosomal dominant and highly penetrant neurodegenerative disorder, results from the pathological expansion (>39) of a polymorphic trinucleotide repeat sequence $(CAG)_n$ within the gene encoding the large, highly conserved protein, huntingtin (HTT) (23). A harmful role for oxidative stress has been described in both HD patients as well as in several experimental models

4

(21, 24) which is potentially due to inherent sensitivity of neurons to damage caused by exposure to an excess of reactive oxygen species (ROS) (25-28). Some anti-oxidant proteins, such as glutathione peroxidases, catalase, and superoxide dismutase (SOD), but not all canonical ARE gene products, are increased in human HD brain (29), suggesting that NRF2 signaling is not fully engaged as a protective mechanism or may be partially repressed. Pharmacological stimulation of NRF2 in HD mouse models is efficacious and associated with increased expression of antioxidant proteins and reduction of ROS levels in brain (30, 31), which further suggests that protective NRF2 signaling is not fully activated and/or muted.

Sustained brain inflammation contributes significantly to the pathogenesis of age-dependent neurodegenerative disorders (32, 33). The release of pro-inflammatory cytokines, associated with the harmful effects of activated microglia in brain, creates a cytotoxic environment for neighboring neurons (34-36). In HD, elevated expression of several key inflammatory mediators is observed in blood, striatum, cortex, and cerebellum from post-mortem patient tissues (37, 38). Neuroinflammatory responses appear relatively early in HD disease progression, suggesting that mutant HTT promotes the abnormal release of cytokines by activated microglia (39-41). The continual release of pro-inflammatory mediators by microglia may perpetuate a feed-forward cycle, recruiting and activating additional microglia, promoting their proliferation, and leading to additional release of pro-inflammatory factors with ever increasing exacerbation of disease pathogenesis (22, 40, 42-45).

It remains uncertain whether NRF2 signaling in human HD is intact or disease-modified and/or differentially impacted in different cell types. Our recent work identified a new structural scaffold of thiazole-containing small molecules that potently induces expression of canonical ARE genes (NQO1, GCLM, GCLC, HMOX1/HO-1) in primary mouse cells and causes a pronounced reduction of reactive oxygen species (46). Here we elucidated the molecular mechanism by which the most potent lead compound developed from this scaffold induces NRF2

5

activation, and used this highly selective probe to examine specific activation responses and potential benefits of NRF2 signaling in mouse and human HD models.

Results

MIND4 is neuroprotective in MPTP-toxicity mouse model

We first sought to evaluate the *in vivo* neuroprotective potential of the new structural scaffold of thiazole-containing NRF2 inducing compounds (46). We tested and established the brain permeability of MIND4 (5-nitro-8-{[5-(phenoxymethyl)-4-phenyl-4H-1,2,4-triazol-3-yl]thio}quinoline), but we were unable to detect the presence in brain of the less hydrophobic analog MIND4-17 (5-nitro-2-{[5-(phenoxymethyl)-4-phenyl-4H-1,2,4-triazol-3-yl]thio}pyridine) (**Fig. 1A, Fig. 2A, Fig. S1**). Studies published to date have shown that NRF2 activation is protective and associated with a reduction in oxidative damage in the 1-methyl-4-phenyl-1,2,3,6-tetrahydropyridine (MPTP) mouse model (47, 48), which was selected for a short-term efficacy trial with MIND4. In a pilot experiment, MIND4 was tested at two different doses in MPTP-treated mice using a subacute treatment paradigm (49). The higher dose of 60 mg/kg attenuated the loss of dopamine and did not change MPTP metabolism significantly (**Fig. 1B, C**). Using the same 60 mg/kg dose and subacute regimen of treatment, we found that MIND4 was protective for dopaminergic neurons in MPTP mice, as demonstrated by an increased level of residual dopamine and a decreased dopamine turnover rate (homovanillic (HVA)/DA) in the drug-treatment group compared to the vehicle-treated control (**Fig. 1D-F**). Furthermore, stereological analysis demonstrated that the MPTP/MIND4-treated mice had more remaining DA neurons in the substantia nigra than the MPTP/vehicle-treated group (**Fig. 1G**). Analysis of pharmacodynamic changes showed that treatment at the selected dose was associated with an increase of antioxidant NRF2-responsive GCLM protein levels, albeit not uniform among the treated animals (n=5) (**Fig. 1H, J**). The levels of acetylated α-tubulin, a prototypic substrate of

SIRT2 deacetylase, identified as a MIND4 target *in vitro*, remained largely unchanged (**Fig. 1I, K**). The results suggest that NRF2 induction contributes to MIND4 protective activity in MPTP-treated mice.

Characterization of thiazole-containing inducers of NRF2 activation

To elucidate the mechanism of NRF2 activation, first we compared the potencies of MIND4, MIND4-17 and a series of structural thiazole-containing analogs in a quantitative NQO1 inducer bioassay in murine Hepa1c1c7 cells (**Fig. 2A, B; Fig. S2A**) (50, 51). The CD value (Concentration which Doubles the specific activity) for NQO1 was used as a measure of inducer potency and compound ranking. Within this lead series, MIND4-17 was confirmed to be the inducer of highest potency (CD = 0.15 µM), comparable to the naturally-occurring inducer sulforaphane (SFP) (CD = 0.18 µM) and significantly more potent than the clinically approved NRF2 activator DMF (CD = 9 µM) (**Fig. 2A, B**) (52-54). A comparative analysis of MIND4-17 and DMF on induction of NRF2-responsive NQO1 and GCLM in mutant HD rat embryonic striatal cells ST14A treated with compounds for 24 h clearly showed higher potency of activation mediated by MIND4-17 (**Fig. 2C**).

As the parent compound MIND4 was initially identified as a SIRT2 inhibitor, activities for this lead series were also tested in a biochemical SIRT2 deacetylation assay (55). In agreement with our previous data (46), there was no correlation between the potencies of SIRT2 inhibition and induction of NQO1; MIND4-17 showed no detectable SIRT2 inhibition activity (**Fig. S2A**).

Next, we established that induction of NQO1 by MIND4-17 and other structural analogs is NRF2-dependent. NQO1 expression was assessed over a series of concentrations in wild-type, NRF2-null, or KEAP1-null mouse embryonic fibroblasts (MEF) after 24 h treatment (56-59). In wild-type MEFs, MIND4-17 exhibited the highest potency, while other MIND4 analogs increased the levels of NQO1 protein to varying degrees (**Fig. S2B**). In contrast, the effects of

MIND4-17 and other MIND4 analogs on induction of NQO1 expression were absent in NRF2-null cells (**Fig. 2D**). In KEAP1-null MEFs, which have constitutively high transcription of NRF2-responsive genes (57, 59), treatment with MIND4-17 and other MIND4 analogs did not upregulate NQO1 expression further (**Fig. S2C**). These results demonstrated that induction of NQO1 expression by MIND4-17 and other structural analogs is NRF2-dependent and KEAP1-dependent.

Stabilization of NRF2 is an essential step of activation of the pathway, which has been well-defined for KEAP1-modifying inducers of NRF2 signaling such as sulforaphane (SFP) (7, 8, 52, 58). Thus we tested whether the stabilization of NRF2 in cells treated with MIND4-17 and its structural analogs preceded the induction of NQO1. Accumulation of total NRF2 protein was readily detectable in wild-type MEFs after 5 h exposure to SFP and MIND4-17 and, to a lesser extent, to the lower potency inducers MIND4 and MIND4B (**Fig. 2E**). In cells treated with MIND4-17, the induction of NQO1 was preceded by nuclear accumulation of NRF2 as early as 30 min after cell exposure to MIND4-17 (0.5 μM) and remained elevated for at least 5 h (**Fig. 2F**).

NRF2 inducing mechanism of MIND4-17

The chemical requirements for the NRF2 inducing activity of MIND4-17 became evident from a structure-activity relationship (SAR) study (**Fig. S3,** please see **Supporting Information** for detailed compound synthesis schemes) (60, 61). Analogs of MIND4-17 with O or C substitutions of the S atom were completely inactive, illuminating the essential requirements for the sulfur for inducer activity (**Fig. S2D-F**). The dependence of inducer activity on an electron-withdrawing group and electron-deficient aromatic system was also apparent (**Fig. S2D-F**). Together, these results suggested that the S group of MIND4-17 could be chemically reactive with cysteine nucleophiles, and that this property is essential for NRF2 activation.

To test this hypothesis, MIND4-17 and other thiazole-containing analogs were pre-

incubated with reduced glutathione (GSH) followed by incubation with intact cells and measurement of NRF2 activation responses. Such pre-treatment negatively affected the ability of MIND4-17 to induce the NRF2 response (**Fig. S2F, G**). Further, pre-incubation with GSH inhibited NRF2 inducer activity in direct correlation with NRF2 activation potency; i.e., MIND4-17 was the most strongly reactive and thus the most profoundly negatively affected. These results indicated that the reactivity of the S group is essential for MIND4-17 mediated activation of NRF2 and involves reaction with cysteine nucleophile(s) of putative target(s).

It is well established that reactive cysteine residues of KEAP1 serve as sensors for electrophiles and oxidants, and that chemical modifications of these cysteines disable the KEAP1/CUL3 complex, ultimately leading to NRF2 activation (7, 11, 12, 53, 62). Located within the BTB domain (Broad complex, Tramtrack and Bric-à-Brac domain), cysteine-151 (C151) is one of the major sensors in KEAP1, the modification of which is sufficient for robust activation of NRF2 (7, 12, 53, 63-65). It was therefore conceivable that C151 of KEAP1 is targeted by MIND4-17. To investigate this possibility, we purified recombinant BTB domain of KEAP1 protein and examined by mass spectrometry its covalent modification in the absence or presence of MIND4-17 (66). The mass for the protein incubated with DMSO (control reaction) was determined to be 16175.6 Da, in good agreement (within <10 ppm) to its calculated mass of 16175.7686 Da (**Fig. 2G**). Incubation of BTB with MIND4-17 resulted in a reduction in the peak for the non-modified protein, and the emergence of a dominant peak at 16298.0 Da, indicating covalent modification of the protein. The observed shift of 122.4 Da was as would be predicted for a single cysteine being modified by formation of a 3-nitropyridine adduct with MIND4-17 (calculated mass difference 123.09 Da).

Next, we validated the putative KEAP1-modyfying mechanism of NRF2 activation by MIND4-17 in live cells (7, 53). COS1 cells were co-transfected with plasmids encoding NRF2-V5 and either KEAP1 wild-type, mutant C151S (cysteine-151 is replaced by serine), or double-mutant C226S/C613S; β-galactosidase was used to monitor transfection efficiencies. In accord

with our previous observations, MIND4-17 stabilized NRF2 in cells expressing wild-type KEAP1 (**Fig. 2H**). In cells expressing a double mutant C226S/C613S KEAP1, MIND4-17 was still able to stabilize NRF2 protein to levels similar to those for wild-type KEAP1 (**Fig. 2H**). In contrast, MIND4-17 failed to stabilize NRF2 in cells expressing the single C151S mutant KEAP1 (**Fig. 2H**). These results therefore were consistent with MIND4-17-dependent activation of NRF2 through a highly selective and covalent modification of the KEAP1 sensor cysteine C151.

To determine if MIND4-17 promiscuously alkylated other reactive cysteines within the proteome, we utilized a quantitative cysteine-reactivity profiling strategy to globally identify cysteine residues that demonstrate significant loss of reactivity upon pre-incubation with compounds (67, 68). Briefly, a promiscuous cysteine reactive iodoacetamide-alkyne (IA) probe coupled to isotopic linkers was used to monitor changes in cysteine reactivity by quantitative mass-spectrometry (MS) (69-71). (For detailed protocol please see **Supporting Information**). Of the >300 reactive cysteine-containing peptides identified in our MS studies, only 4 residues showed a >2-fold change in cysteine reactivity upon treatment with MIND4-17 (**SI Dataset**). Within the subset of cysteines with no change in reactivity were hyper-reactive cysteine residues such as the active-site nucleophile of GAPDH, attesting to the low reactivity of the MIND4-17 across even highly reactive cysteines within the proteome.

MIND4-17 causes conformational change in the KEAP1:NRF2 protein complex in live cells

We further validated the MIND4-17 mechanism of NRF2 activation using a recently developed FRET/FLIM methodology (14, 72) and examined whether MIND4-17 treatment arrests the KEAP1/NRF2 complex in the *closed* conformation, thus permitting *de novo* NRF2 accumulation and translocation in nuclei to activate ARE-gene transcription. The effects of MIND4-17 on the conformational changes of the KEAP1:NRF2 complex were determined in HEK293 cells ectopically expressing fluorescent EGFP-NRF2 and KEAP1-mCherry fusion proteins, or EGFP-NRF2 and free mCherry as a negative control. As expected, in vehicle-treated

cells transfected with EGFP-NRF2 and free mCherry, most of the NRF2 was in the nucleus (**Fig. 3A, first row, images**), and the lifetime of EGFP fluorescence in the cytoplasm was 2324 ± 7 ps (n=6) (**Fig. 3A, first row, graph**). When KEAP1-mCherry was co-expressed with EGFP-NRF2, NRF2 was largely cytoplasmic (**Fig. 3A, second row, images**), and the EGFP lifetime was significantly reduced to 2184 ± 42 ps (n=6, p=1.14E-05) (**Fig. 3A, second row, graph**), indicating the occurrence of FRET between the fluorophores and demonstrating that the two fusion proteins interact. No significant changes were observed in the sub-cellular localization of EGFP-NRF2 upon addition of MIND4-17 to cells co-expressing EGFP-NRF2 and free mCherry (**Fig. 3A, third row, images and graph**). In contrast, exposure to 1 μM of MIND4-17 for 1 h promoted the nuclear accumulation of EGFP-NRF2 in cells co-expressing EGFP-NRF2 and KEAP1-mCherry (**Fig. 3A, fourth row, images)**, and the EGFP lifetime was significantly reduced further to 2147 ± 50 ps (n=17, p=5.98E-09) (**Fig. 3A, fourth row, graph)**.

Further quantification of the FRET efficiency revealed that, in the cytoplasm of vehicle-treated cells, 62% of the KEAP1:NRF2 complex was in the *open* conformation, and 38% in the *closed* conformation. Treatment with MIND4-17 inverted this ratio to 44% and 56% of KEAP1:NRF2 complexes being in the *open* and the *closed* conformations, respectively (**Fig. 3B**). These results obtained by FRET/FLIM analysis in live cells showed that MIND4-17 arrests the NRF2:KEAP1 protein complex in the *closed* conformation, which is similar to previously reported effects of the electrophilic NRF2 inducers sulforaphane and sulfoxythiocarbamate alkyne (13) but in contrast to the effects of the non-electrophilic triazole inducer HB229, which directly disrupts the KEAP1:NRF2 protein:protein interaction (73).

Taken together, these data delineate a mechanism of NRF2 activation by MIND4-17 through specific covalent modification of KEAP1 sensor-cysteine C151, subsequently causing accumulation and nuclear translocation of *de novo* synthesized NRF2, and activation of NRF2-dependent gene transcription. Thus, MIND4-17 acts as a highly KEAP1-selective stress-

mimicking compound (74), and was next employed for investigating NRF2 signaling responses in HD models systems.

NRF2 activation by MIND4-17 induces anti-inflammatory effects in microglia and macrophages

NRF2 activation-dependent anti-inflammatory responses have been well described in microglia cells (75, 76). It has been also shown that genetic or pharmacologic NRF2 activation counteracts release of pro-inflammatory cytokines in the context of exposure to UV radiation (20). Thus, we first validated the effect of MIND4-17 treatment on repression of pro-inflammatory cytokines in microglial cells and also in peripheral macrophages which are known to infiltrate CNS in late-stage HD. As expected, treatment of mouse microglial BV2 cells with MIND4-17 resulted in a potent and concentration-dependent increases in transcription of the canonical ARE genes *GCLM* and *NQO1* in both resting and lipopolysaccharide (LPS)-activated microglial cells (**Fig. 4A, B**). Concomitantly, treatment with MIND4-17 resulted in a concentration-dependent repression of the pro-inflammatory factors *IL-6*, *IL-1β*, *TNFα*, and *MCP-1* (**Fig. 4C-F**). MIND4-17 treatment similarly repressed *IL-6*, *IL-1β*, *TNFα*, and *MCP-1* and activated *NQO1* and *GCLM* genes in resting and LPS-stimulated bone marrow-derived macrophages (**Fig. S4**) (77).

Anti-inflammatory NRF2 activation response in HD and wild-type primary mouse microglia and astrocytes

Having established that MIND4-17 represses cytokine expression, next we probed for anti-inflammatory effects of NRF2 activation in brain-resident non-neuronal cells, namely microglia and astrocytes, and specifically examined the effect on release of IL-6, an established marker of inflammation in HD model systems (40, 78).

MIND4-17 was first evaluated for its impact on inflammatory responses in primary

12

microglia derived from wild-type and HD mutant YAC128 mice (79). The YAC128 mouse model of HD expresses the full-length human transgene with 128 CAG repeats and replicates key elements of HD phenotypes and selective neurodegeneration. Previous studies in peripheral blood monocytes from YAC128 mice focused on IL-6 as a marker of inflammation in HD (80). Release of IL-6 from wild-type and YAC128 microglia was induced by stimulation with control standard endotoxin (CSE) and INF-γ. MIND4-17 reduced the amount of IL-6 secreted from wild-type and YAC128 primary microglia in a concentration-dependent manner and in highly similar fashion (**Fig. 4G**). Experiments were next extended to primary astrocytes derived from wild-type and YAC128 mice. MIND4-17 treatment resulted in a similar concentration-dependent reduction of IL-6 release in CSE-stimulated primary astrocytes derived from YAC128 and wild-type mice (**Fig. 4H**).

Taking advantage of the brain permeability of the MIND4 analog, which, similar to MIND4-17, repressed cytokine expression in LPS-induced microglia (**Fig. S4G**), we next conducted a semi-acute 2-week treatment of symptomatic HD R6/2 mice (81). A statistically significant reduction of cortical TNFα levels was detected (**Fig. S4H-K**), consistent with the anti-inflammatory effects of the NRF2 activation observed in primary mouse microglia and astrocytes (**Fig. 4G, H**) These results suggest that the anti-inflammatory NRF2 activation response remains available for induction in symptomatic R6/2 mice with well-progressed HD neurological phenotype. Interestingly, cortical TNFα levels were not significantly different between untreated wild type and R6/2 mice (**Fig. S4, J**), suggesting the TNFα itself is unlikely to be the sole driver of neuroinflammation in HD.

Anti-inflammatory NRF2 activation responses are intact in primary monocytes from HD patients

Finally, to validate these HD model results in human HD, the anti-inflammatory effects of NRF2 induction by MIND4-17 were examined in primary human monocytes derived from HD patients

13

and non-disease controls. *Ex vivo* peripheral immune cells from HD patients produce significantly more pro-inflammatory cytokines in response to LPS and INF-γ stimulation than cells isolated from control subjects (40, 78). Here, we induced production of the pro-inflammatory cytokines IL-1, IL-6, IL-8, and TNFα in primary monocytes by stimulation with LPS and INF-γ. Pre-treatment with MIND4-17, prior to induction with LPS/ INF-γ significantly decreased the levels of all four pro-inflammatory cytokines in both HD and control monocytes (**Fig. 5, Fig. S5A-D**). In HD monocytes, MIND4-17 significantly repressed the expression of all four cytokines at the 3 µM and 1 µM concentrations and repressed IL-8 and TNFα expression at the lowest tested concentration of 0.3 µM, demonstrating a highly similar pattern of the compound effects in the disease and non-disease counterparts. Neither vehicle (DMSO) nor MIND4-17 affected the viability of primary human monocytes at any of the concentrations tested (**Fig. S5E**).

The responses in human monocytes were consistent with the effects observed in the mouse models. Overall, the results suggest that NRF2 activation in non-neuronal primary HD cells is intact, amenable to activation, and capable to mediate anti-inflammatory protective responses.

NRF2 activation responses are muted in human HD neural stem cells

We next evaluated NRF2 activation responses in experimental neural HD models of human origin. Nestin-positive HD48 (mutant 42CAG) and HD51 (mutant 51CAG) and non-disease WT55 and WT54 neural stem cells (NSCs) were differentiated from human iPSCs, based on a protocol described for mouse ES cells (82) (**Fig. S6**; please see **Supporting Information** for detailed protocols). Cells were treated for 24 h with MIND4-17 at a concentration range of 0.1-3 µM, and levels of the canonical NRF2-responsive proteins NQO1 and GCLM (**Fig. 6A)** and HTT (**Fig. 6B**) were examined by immunoblotting. The levels of NQO1 were significantly higher in both HD cell lines and thus a lower amount of protein per lane was loaded to illuminate the compound effects (**Fig. 6C**; note multiple NQO1 molecular weight bands reflecting known

14

protein isoforms). Treatment with MIND4-17 induced a concentration-dependent increase of the NRF2-responsive proteins NQO1 and GCLM in HD and non-disease cells. The MIND4-17-dependent increase of NQO1 and GCLM levels started at 1 μM in both HD and at 0.1 μM in both non-disease cell lines. MIND4-17 treatment had no detectable effects on HTT levels.

To determine if the magnitude of NRF2 response varied in HD versus non-disease cells, we compared the maximum fold-induction of NQO1 expression. A maximal ~2-fold response was observed in each HD cell line at 3 μM of MIND4-17 (**Fig. 6D, E**). Non-disease WT cells showed a maximum ~4-fold response at 1 μM of MIND4-17, which plateaued by 3 μM (**Fig. 6D, E**). These data suggest that NRF2 induction could be compromised in HD due to suppressive influence of the expanded CAG repeat mutation on pathway activation; alternatively, a reduced fold-change in response to MIND4-17 could be due to a pre-existing partial or full activation in response to mHTT-induced homeostatic changes in the HD cells.

To distinguish between these two possibilities, we compared responses in NSC HD4 with a severe 72 CAG mutation and its isogenic-counterpart NSC HD116c, in which the 72 CAG expansion was corrected to a non-pathological 21 CAG repeat length by homologous recombination (83). In HD4 NSCs the basal levels of NQO1 and GCLM proteins were similar to HD116c (**Fig. 6F**), indicating the NRF2 pathway was not partially activated. Treatment with MIND4-17 did not induce a significant increase of either NQO1 or GCLM expression in HD4 cells (**Fig. 6G, I, J**). In sharp contrast, MIND4-17 treatment induced a concentration-dependent increase of NQO1 and GCLM expression in HDc116 cells (**Fig. 6H, K**), similar to that observed in WT54 and WT55 NSCs (**Fig. 6A**). The induction of both NRF2-responsive proteins in the corrected HDc116 cells was significant at 0.3 μM concentration of MIND4-17. A maximum 4-fold response was observed at concentrations 1 and 3 μM, which was similar to the response in non-disease NSCs.

Together, these data show that the HD mutation negatively impacts NRF2 signaling and

suggest that interference is even greater for the extreme CAG pathological expansions, which are associated with juvenile clinical cases.

Discussion

In the present study we have developed and determined the mechanism of action of a novel and highly selective small molecule inducer of NRF2 signaling, MIND4-17. The NRF2 signal transduction cascade is initiated by MIND4-17 through highly selective, covalent modification of the KEAP1 sensor-cysteine C151, mimicking effects of oxidative and electrophilic stress (10, 12, 53, 63). This chemical modification of KEAP1 leads to conformational change and arrest of the KEAP1/NRF2 complex in the *closed* conformation, disrupting the cycle of degradation of NRF2 (13, 66, 74). Subsequently, this results in accumulation (stabilization) and nuclear translocation of *de novo*-synthesized NRF2, followed by NRF2-mediated activation of gene expression. Proteomic analysis showed high MIND4-17 selectivity for the KEAP1 target, which makes this compound an attractive probe for investigating the activation of NRF2 signaling (74).

A highly specific KEAP1-modyfing inducer probe such as MIND4-17 has key advantages over genetic manipulations or broadly unspecific oxidants or electrophiles for investigating endogenous biological responses specific to NRF2 signaling in stress. For example, the gene silencing of KEAP1, whose expression is NRF2-dependent, would disrupt an auto-regulatory loop (84) and, due to the absence of natural formation of the substrate adaptor and E3 ubiquitin ligase KEAP1/CUL3 complex, would result in over-activation of the NRF2 pathway (47). Moreover, in contrast to small organic inducers like DMF and SFP, which lack selectivity and "SAR-ability," the novel MIND4-17 scaffold presented here is drug-like and amenable to further chemical modifications to optimize its pharmaceutical properties. In this context, a key pharmacokinetic property requiring further optimization will be brain permeability, which is minimal for MIND4-17 itself and precludes its direct consideration as a clinical candidate.

While mutant HTT is ubiquitously expressed and impacts multiple cell types across all bodily tissues, we next investigated NRF2 signaling in the non-neuronal cell populations that are the principal mediators of neuroinflammation, namely, microglia, astrocytes and peripheral monocytes, and in the context of both mouse and human HD model systems. Our results showed that the selective NRF2 inducer MIND4-17 repressed expression of pro-inflammatory cytokines in primary microglia and astrocytes from HD and wild-type mice (40, 78). Similar effects were observed in human primary monocytes from HD patients and normal subjects, in which MIND4-17 mediated repression of pro-inflammatory cytokines in both disease and non-disease cells. Based on these results, we concluded that NRF2 and downstream anti-inflammatory pathways are intact and not affected by the HD mutation in these non-neuronal populations.

This finding is especially important as dysfunction in non-neuronal cell types is recognized as a potential contributor to neurodegeneration, in which a critical role for activated microglia in HD has emerged (85). The release of pro-inflammatory cytokines, associated with the harmful effects of activated microglia in brain, creates a cytotoxic environment for neighboring neurons (34-36). The potential therapeutic benefits of NRF2 activation are increasingly appreciated to originate in glial and CNS-relevant immune cells including microglia and peripheral macrophages (86). Thus, the results from our studies highlight the therapeutic potential of NRF2 signaling to repress pro-inflammatory processes in the brain parenchyma including astroglia, microglia, and infiltrating peripheral macrophages.

NRF2 activation responses were evaluated in human NSCs derived from patient iPSCs. NSCs can give rise to neurons, astrocytes, oligodendroglia and in HD exhibit phenotypes that may be pathologically relevant (83, 87). Moreover, there is evidence that the pool of adult NSCs is depleted in the striatum of HD patient brains (88) and may further contribute to HD pathology over time. Our results showed that in HD NSCs with a CAG repeat expansion in the range typical for adult-onset disease, NRF2 responses were muted compared to non-disease counterparts. Induction of NRF2 responses were essentially silent in NSCs with an extreme CAG repeat length

associated with juvenile onset, but were restored to non-disease levels upon isogenic genetic correction of the CAG expansion. Our data showed that in the context of human HD NSCs, NRF2 signaling is muted, which was consistent with similar observation in the striatal STHdh mHTT Q111/Q111 cell line (89), although it is yet unclear whether mHTT is directly involved. The results imply a high stress-sensitivity of HD NSCs in adult brain, which could offer an explanation for depletion of these cells in the course of disease (88).

Taken together, our results highlight a differential and complex NRF2-dependent stress-response in human brain and emphasize potential therapeutic benefits of NRF2 activation for HD treatment.

Materials and Methods

Compound source and storage

Compounds were procured from ChemBridge Corp. San Diego (purity QC ensured by provided NMR spectroscopy data), dissolved in molecular biology grade dimethyl sulfoxide (DMSO) to 10 mM stock concentrations, aliquoted, and stored at -80°C. MIND4-17 was re-synthesized (purity >95%) and showed essentially identical potency of NRF2 activation to MIND4-17 in multiple batches purchased from ChemBridge. Design and schemes for synthesis of MIND4-17 analogs 2872, 2286, 2291, 2907, and 2909 can be can be found in **Supporting Information**. Dimethyl fumarate was purchased from Sigma and sulforaphane from LKT Laboratories, Inc.

Drug test in MPTP mouse model

MIND4 was solubilized at 5mg/ml in 7.5% Cremophor EL (BASF)/2.375% Ethanol in PBS. Please see **Supporting Information** for details on tolerability and brain-permeability studies. Male C57BL/6 mice (~25 g) from Charles River Laboratories, Wilmington, MA were housed in temperature- and humidity-controlled rooms with a 12 h dark: light cycle and had free access to food and water. Subacute MPTP paradigm (20 mg/kg i.p. injection once daily for 4 days) was employed to test dose response of MIND4 (90) at 30 mg/kg or 60 mg/kg, (i.p. 10min before and

50min after each MPTP injection). The effective dose of 60 mg/kg was used in the subsequent experiments. Control animals received saline (control for MPTP) and 10% propylene glycol and 90% dextrose as vehicle for MIND4 by i.p. Mice were sacrificed 7 days after the last MPTP administration and striatal DA and metabolite HVA were determined by high performance liquid chromatography (HPLC) coupled with electrochemical detection (ECD) (90). Immunostaining for tyrosine hydroxylase (TH), a marker for dopaminergic neurons was performed using mouse anti-TH antibody (Sigma, ST. Louis, MO). Total numbers of TH positive neurons in the substantia nigra (SN) were counted under blinded conditions using the Bioquant Image Analysis System (R&M Biometrics, Nashville, TN) (91).

NQO1 bioassay

Inducer potency was quantified by use of the NQO1 bioassay in Hepa1c1c7 cells as described (50, 51). In brief, cells grown in 96-well plates were exposed to serial dilutions of each compound for 48 h, and the NQO1 enzyme activity was determined in cell lysates. Results are shown as average values of 8 replicate wells. The standard deviation in each case was less than 5%.

Compound activity test in the rat embryonic striatal cell lines ST14A

ST14A cells (a generous gift of E. Cattaneo) (92) stably express either a mutant expanded repeat (128Q) or wild-type (26Q) 546 amino acid huntingtin (HTT) fragment and were treated with compounds for 24 h as described (93). Please see **Supporting Information** for information on antibodies.

Compound activity test in mouse embryonic fibroblasts

Mouse embryonic fibroblasts (MEFs) from wild-type (WT), NRF2-knockout (NRF2-KO) or KEAP1-knockout (KEAP1-KO) mice (59) were cultured in plastic dishes (Invitrogen) coated for 30 min with 0.1% (w/v) gelatin. For experiments, cells (250,000 per well) were grown for 24 h on 6-well plates, and then treated with solvent control (0.1% DMSO, v/v) or compounds for 24 h. For Western blot analysis cells were lysed in RIPA buffer, containing 1 protease inhibitor cocktail tablet (Roche) per 10 mL buffer. Proteins were resolved by SDS-PAGE and

19

immunoblotted with specific antibodies against NQO1 (1:1000) or NRF2 (1:1000), both gifts from Professor John D. Hayes, University of Dundee, and β-actin (Sigma, mouse monoclonal, 1:10000). Conventional method was used to separate nuclear and cytoplasmic fractions to test NRF2 induction and stabilization (please see **Supporting Information** for details).

Cell-based KEAP1-target validation assay

COS1 cells were plated 16 h before transfection, followed by co-transfection with plasmids encoding wild-type, mutant C151S, or C226S/C613S double-mutant KEAP1 and NRF2-V5 (generous gifts from Dr. M. MacMahon and Professor John D. Hayes, University of Dundee) at 1:1 ratios. A plasmid encoding β-galactosidase was co-transfected to monitor transfection efficiency. 24 h post-transfection, cells were exposed to MIND4-17 for 3 h, extracts were prepared and loaded on SDS-PAGE normalized by β-galactosidase activity. Samples were resolved on SDS-PAGE and immunoblotted with antibodies against KEAP1 (1:2000, rabbit polyclonal, a kind gift from Professor John D. Hayes, University of Dundee) and V-5 (1:5000, mouse monoclonal, Invitrogen).

Fluorescence lifetime imaging analysis of NRF2:KEAP1 complex

HEK293 cells (200,000 per dish) grown in standard media in 6 cm glass dishes were co-transfected with constructs encoding EGFP-NRF2 and KEAP1-mCherry using Lipofectamine 2000 (Invitrogen) as described (13). Cells were imaged 24 h post-transfection before and after 1 h exposure to 1 μM MIND4-17. All images were acquired by confocal microscopy using a laser-scanning confocal microscope (LSM780; Carl Zeiss). The microscope was equipped with a thermostatic chamber suitable to maintain the live cells and optics at constant 37°C. Imaging was performed using a 63x oil immersion NA 1.4 Plan-Apochromat objective from Zeiss. Fluorescence lifetime imaging microscopy (FLIM) was performed as described (94). Specific details of analysis are provided in **Supporting Information**.

Mass spectrometry analysis of KEAP1 modification(s)

Expression and purification of recombinant BTB and full-length KEAP1 proteins are described in details in the **Supporting Information**. To analyze covalent modification(s) of the BTB domain, 10 μM BTB [48-190 S182A] were incubated with 2 mM MIND4-17 (or 2% DMSO final concentration for control) for 1 h on ice in 20 mM Tris-HCl pH 8.0, 150 mM NaCl. Intact protein masses were determined through HPLC-coupled ESI-MS on an AB Sciex TripleTOF 5600+ mass spectrometer (Sciex) as described in detail in **Supporting Information**.

NRF2-dependent transcriptional profiling of MIND4-17 in BV2 microglia cells

The BV2 mouse microglial cell line was a generous gift from Dr. Michael Whalen (Massachusetts General Hospital). Cells were maintained in DMEM media (Invitrogen) supplemented with 10% FBS (Sigma) and antibiotic-antimycotic mix (Invitrogen). Cells were seeded into 12-well plates at the density of 3×10^5 cells/well. Cells were treated with the indicated concentrations of MIND4-17 for 24 h. Cells were then stimulated with 10 ng/ml LPS (E.coli, Sigma) for 2 h. Total RNA was isolated using ZR Miniprep kit (Zymo Research). 1 mg of total RNA was used to prepare cDNA (ProtoScript kit, New England Biolabs). Gene expression levels for *NQO1, GCLM, IL1, IL6, TNFα, and MCP1* were analyzed by the VeriQuest SYBR green assay (Affymetrix) using a Roche480 thermocycler. The sequences of gene-specific primers for qPCR can be found in the **Supporting Information**.

MIND4-17 activity test on cytokine IL-6 release in primary mouse astrocytes and microglia

Whole brains were obtained from postnatal 1 to 3 d old wild-type and YAC128 mouse pups on the FVB/N strain background and placed in Hank's Balanced Salt Solution (Invitrogen) on ice. Meninges were removed and the remaining brain tissue was placed into growth medium (DMEM, 10% FBS, 1% L-glutamine, 1% penicillin/streptomycin), and homogenized. Please see details on cell isolation and culturing in **Supporting Information**. After the initial isolation microglia and astrocytes were seeded at a density of 1.4×10^5 cells/ml into 96-well tissue culture plates. 24 h later, the culture media was replaced with media containing MIND4-17 at different concentrations in growth medium containing 1% FBS. 24 h later medium containing interferon-γ

(INF-γ; final concentration 10 ng/ml; R&D Systems) with CSE (Control Standard Endotoxin, Associates of Cape Cod) at a final concentration 100 ng/ml. Supernatants were collected at 9 h, and stored at -20°C. Cells were lysed and total protein levels were determined using the micro BCA kit (Thermo Scientific). Supernatants were analyzed using mouse IL-6 ELISA (e-Biocience) and IL-6 levels normalized to total protein levels.

MIND4-17 activity test on cytokine expression in primary human HD and non-disease monocytes

All human experiments were performed in accordance with the Declaration of Helsinki and approved by University College London (UCL)/UCL Hospitals Joint Research Ethics Committee. All subjects provided informed written consent. Blood samples were obtained from control subjects and genetically-diagnosed, symptomatic HD patients. Patients were classed as having early or moderate-stage disease using the total functional capacity (TFC) scale (13-7, early; 6-3, moderate) (95). Subjects with inflammatory or infective conditions were excluded.

Information on cohorts of HD and healthy subjects participated in the study:

HD (n=13): age=56.84 +/- 9.23; CAG repeats= 42.46 +/- 1.80; female/male ratio=53/47. Healthy subjects (n=10): age=49.98 +/- 15.03; female/male ratio=53/47.

Cells were isolated from whole blood, as previously described (40). (Please see **Supporting Information** for details). After resting for 16 h, the culture media was replaced with R10 media containing either vehicle (DMSO) or MIND4-17 at different concentrations (0.3, 1, and 3 μM). After 24 h treatment, media was changed again using R10 containing both MIND4-17 at the same concentration and, to stimulate cytokine production, 10 ng/ml INF-γ (R&D Systems) and 2 mg/ml lipopolysaccharide (LPS, Sigma-Aldrich). Supernatants were collected at 24 h and analyzed using the human pro-inflammatory II (4-plex) MSD assay measuring IL-1β, IL-6, IL-8 and TNFα. Normalized cytokine levels were analyzed on a logarithmic scale due to their skewed distribution. Statistical analysis was performed using a linear mixed model, to allow for correlation between measurements from the same subject. A constant correlation was assumed between all 6 measurements from each subject, with robust standard errors to allow for deviation

from this assumption. An advantage of this approach is that linear mixed models provided unbiased estimates of each comparison even if there were missing data, provided the data was assumed to be missing at random. Contrasts of interest were then calculated using linear combinations of parameter estimates.

MIND4-17 activity test in human neuronal stem cells (NSCs)

iPSCs were obtained from NINDS Repository at the Coriell Institute for Medical Research: Cat# ND38554 (named here WT54); Cat# ND3855 (WT55); Cat# ND38551 (HD51); Cat# ND38548 (HD48). The HD4 cell line harbors a severe juvenile repeat range 72 CAG mutation; in the isogenic-companion cell line HD116c the pathological mutant CAG expansion was corrected to a non-pathological 21 CAG repeat by homologous recombination (83). Genotype was confirmed by PCR amplification of genomic DNA (**Fig. S6A**). Please see **Supporting Information** for additional details on maintenance iPSCs. NSCs were established based on a protocol described for mouse ES cells (82) and detailed protocol is provided in **Supporting Information.** For compound treatments, cells were plated at 100,000 cells/well on poly-L-lysine/laminin coated 24-well plates. Compound was diluted to 2x the final concentration in complete medium then an equal volume of solution was added to each well. The final concentrations of MIND4-17 were 0-3 μM. An equal volume of carrier (DMSO) was used as a control. Cells were treated for 24 h then lysed in buffer and analyzed by SDS-PAGE and Western blot.

Acknowledgments

References

1.   Itoh, K., Wakabayashi, N., Katoh, Y., Ishii, T., Igarashi, K., Engel, J. D., & Yamamoto, M. (1999) *Genes & development* 13, 76-86.

2.   Kensler, T. W., Wakabayashi, N., & Biswal, S. (2007) *Annual review of pharmacology and toxicology* 47, 89-116.

3.   Baird, L. & Dinkova-Kostova, A. T. (2011) *Archives of toxicology* 85, 241-272.

4.   Cullinan, S. B., Gordan, J. D., Jin, J., Harper, J. W., & Diehl, J. A. (2004) *Molecular and cellular biology* 24, 8477-8486.

5.   Tong, K. I., Kobayashi, A., Katsuoka, F., & Yamamoto, M. (2006) *Biological chemistry* 387, 1311-1320.

6.   Tong, K. I., Padmanabhan, B., Kobayashi, A., Shang, C., Hirotsu, Y., Yokoyama, S., & Yamamoto, M. (2007) *Molecular and cellular biology* 27, 7511-7521.

7.   Zhang, D. D. & Hannink, M. (2003) *Molecular and cellular biology* 23, 8137-8151.

8.   McMahon, M., Itoh, K., Yamamoto, M., & Hayes, J. D. (2003) *The Journal of biological chemistry* 278, 21592-21600.

9.   Zhang, D. D., Lo, S. C., Cross, J. V., Templeton, D. J., & Hannink, M. (2004) *Molecular and cellular biology* 24, 10941-10953.

10.   Kobayashi, A., Kang, M. I., Okawa, H., Ohtsuji, M., Zenke, Y., Chiba, T., Igarashi, K., & Yamamoto, M. (2004) *Molecular and cellular biology* 24, 7130-7139.

11.   Dinkova-Kostova, A. T., Holtzclaw, W. D., Cole, R. N., Itoh, K., Wakabayashi, N., Katoh, Y., Yamamoto, M., & Talalay, P. (2002) *Proceedings of the National Academy of Sciences of the United States of America* 99, 11908-11913.

12.   McMahon, M., Lamont, D. J., Beattie, K. A., & Hayes, J. D. (2010) *Proceedings of the National Academy of Sciences of the United States of America* 107, 18838-18843.

13.   Baird, L., Lleres, D., Swift, S., & Dinkova-Kostova, A. T. (2013) *Proceedings of the National Academy of Sciences of the United States of America* 110, 15259-15264.

14. Baird, L. & Dinkova-Kostova, A. T. (2013) *Biochemical and biophysical research communications* 433, 58-65.

15. Lee, J. M., Calkins, M. J., Chan, K., Kan, Y. W., & Johnson, J. A. (2003) *The Journal of biological chemistry* 278, 12029-12038.

16. Hayes, J. D. & Dinkova-Kostova, A. T. (2014) *Trends in biochemical sciences* 39, 199-218.

17. Kobayashi, E. H., Suzuki, T., Funayama, R., Nagashima, T., Hayashi, M., Sekine, H., Tanaka, N., Moriguchi, T., Motohashi, H., Nakayama, K*., et al.* (2016) *Nature communications* 7, 11624.

18. Liu, H., Dinkova-Kostova, A. T., & Talalay, P. (2008) *Proceedings of the National Academy of Sciences of the United States of America* 105, 15926-15931.

19. Lee, D. H., Gold, R., & Linker, R. A. (2012) *Int J Mol Sci* 13, 11783-11803.

20. Knatko, E. V., Ibbotson, S. H., Zhang, Y., Higgins, M., Fahey, J. W., Talalay, P., Dawe, R. S., Ferguson, J., Huang, J. T., Clarke, R*., et al.* (2015) *Cancer prevention research (Philadelphia, Pa* 8, 475-486.

21. Browne, S. E. & Beal, M. F. (2006) *Antioxid Redox Signal* 8, 2061-2073.

22. Moller, T. (2010) *J Neural Transm* 117, 1001-1008.

23. Group, T. H. s. D. C. R. (1993) *Cell* 72, 971-983.

24. Sorolla, M. A., Rodriguez-Colman, M. J., Vall-llaura, N., Tamarit, J., Ros, J., & Cabiscol, E. (2012) *BioFactors (Oxford, England)* 38, 173-185.

25. Stack, E. C., Matson, W. R., & Ferrante, R. J. (2008) *Annals of the New York Academy of Sciences* 1147, 79-92.

26. Li, X., Valencia, A., Sapp, E., Masso, N., Alexander, J., Reeves, P., Kegel, K. B., Aronin, N., & Difiglia, M. (2010) *J Neurosci* 30, 4552-4561.

27. Johri, A. & Beal, M. F. (2012) *Biochimica et biophysica acta* 1822, 664-674.

28. Tsunemi, T., Ashe, T. D., Morrison, B. E., Soriano, K. R., Au, J., Roque, R. A., Lazarowski, E. R., Damian, V. A., Masliah, E., & La Spada, A. R. (2012) *Science translational medicine* 4, 142ra197.

29. Sorolla, M. A., Reverter-Branchat, G., Tamarit, J., Ferrer, I., Ros, J., & Cabiscol, E. (2008) *Free radical biology & medicine* 45, 667-678.

30. Ellrichmann, G., Petrasch-Parwez, E., Lee, D. H., Reick, C., Arning, L., Saft, C., Gold, R., & Linker, R. A. (2011) *PloS one* 6, e16172.

31. Stack, C., Ho, D., Wille, E., Calingasan, N. Y., Williams, C., Liby, K., Sporn, M., Dumont, M., & Beal, M. F. (2010) *Free radical biology & medicine* 49, 147-158.

32. Bonifati, D. M. & Kishore, U. (2007) *Molecular immunology* 44, 999-1010.

33. Pizza, V., Agresta, A., D'Acunto, C. W., Festa, M., & Capasso, A. (2011) *CNS & neurological disorders drug targets* 10, 621-634.

34. Nagatsu, T. & Sawada, M. (2005) *Current pharmaceutical design* 11, 999-1016.

35. Phani, S., Loike, J. D., & Przedborski, S. (2012) *Parkinsonism & related disorders* 18 Suppl 1, S207-209.

36. Smith, J. A., Das, A., Ray, S. K., & Banik, N. L. (2012) *Brain research bulletin* 87, 10-20.

37. Dalrymple, A., Wild, E. J., Joubert, R., Sathasivam, K., Bjorkqvist, M., Petersen, A., Jackson, G. S., Isaacs, J. D., Kristiansen, M., Bates, G. P.*, et al.* (2007) *Journal of proteome research* 6, 2833-2840.

38. Silvestroni, A., Faull, R. L., Strand, A. D., & Moller, T. (2009) *Neuroreport* 20, 1098-1103.

39. Sapp, E., Kegel, K. B., Aronin, N., Hashikawa, T., Uchiyama, Y., Tohyama, K., Bhide, P. G., Vonsattel, J. P., & DiFiglia, M. (2001) *Journal of neuropathology and experimental neurology* 60, 161-172.

40. Bjorkqvist, M., Wild, E. J., Thiele, J., Silvestroni, A., Andre, R., Lahiri, N., Raibon, E., Lee, R. V., Benn, C. L., Soulet, D*., et al.* (2008) *The Journal of experimental medicine* 205, 1869-1877.

41. Wild, E., Magnusson, A., Lahiri, N., Krus, U., Orth, M., Tabrizi, S. J., & Bjorkqvist, M. (2011) *PLoS currents* 3, RRN1231.

42. Pavese, N., Gerhard, A., Tai, Y. F., Ho, A. K., Turkheimer, F., Barker, R. A., Brooks, D. J., & Piccini, P. (2006) *Neurology* 66, 1638-1643.

43. Tai, Y. F., Pavese, N., Gerhard, A., Tabrizi, S. J., Barker, R. A., Brooks, D. J., & Piccini, P. (2007) *Brain research bulletin* 72, 148-151.

44. Frank-Cannon, T. C., Alto, L. T., McAlpine, F. E., & Tansey, M. G. (2009) *Molecular neurodegeneration* 4, 47.

45. Politis, M., Pavese, N., Tai, Y. F., Kiferle, L., Mason, S. L., Brooks, D. J., Tabrizi, S. J., Barker, R. A., & Piccini, P. (2011) *Human brain mapping* 32, 258-270.

46. Quinti, L., Casale, M., Moniot, S., Pais, T. F., Van Kanegan, M. J., Kaltenbach, L. S., Pallos, J., Lim, R. G., Naidu, S. D., Runne, H*., et al.* (2016) *Cell Chemical Biology*.

47. Williamson, T. P., Johnson, D. A., & Johnson, J. A. (2012) *Neurotoxicology* 33, 272-279.

48. Kaidery, N. A., Banerjee, R., Yang, L., Smirnova, N. A., Hushpulian, D. M., Liby, K. T., Williams, C. R., Yamamoto, M., Kensler, T. W., Ratan, R. R*., et al.* (2013) *Antioxid Redox Signal* 18, 139-157.

49. Bezard, E. & Przedborski, S. (2011) *Mov Disord* 26, 993-1002.

50. Prochaska, H. J. & Santamaria, A. B. (1988) *Analytical biochemistry* 169, 328-336.

51. Fahey, J. W., Dinkova-Kostova, A. T., Stephenson, K. K., & Talalay, P. (2004) *Methods in enzymology* 382, 243-258.

52. Zhang, Y., Talalay, P., Cho, C. G., & Posner, G. H. (1992) *Proceedings of the National Academy of Sciences of the United States of America* 89, 2399-2403.

53. Takaya, K., Suzuki, T., Motohashi, H., Onodera, K., Satomi, S., Kensler, T. W., & Yamamoto, M. (2012) *Free radical biology & medicine* 53, 817-827.

54. Fox, R. J., Kita, M., Cohan, S. L., Henson, L. J., Zambrano, J., Scannevin, R. H., O'Gorman, J., Novas, M., Dawson, K. T., & Phillips, J. T. (2014) *Current medical research and opinion* 30, 251-262.

55. Outeiro, T. F., Kontopoulos, E., Altmann, S. M., Kufareva, I., Strathearn, K. E., Amore, A. M., Volk, C. B., Maxwell, M. M., Rochet, J. C., McLean, P. J*., et al.* (2007) *Science* 317, 516-519.

56. Wakabayashi, N., Itoh, K., Wakabayashi, J., Motohashi, H., Noda, S., Takahashi, S., Imakado, S., Kotsuji, T., Otsuka, F., Roop, D. R*., et al.* (2003) *Nature genetics* 35, 238-245.

57. Wakabayashi, N., Dinkova-Kostova, A. T., Holtzclaw, W. D., Kang, M. I., Kobayashi, A., Yamamoto, M., Kensler, T. W., & Talalay, P. (2004) *Proceedings of the National Academy of Sciences of the United States of America* 101, 2040-2045.

58. Benedict, A. L., Knatko, E. V., & Dinkova-Kostova, A. T. (2012) *Carcinogenesis* 33, 2457-2466.

59. Ludtmann, M. H., Angelova, P. R., Zhang, Y., Abramov, A. Y., & Dinkova-Kostova, A. T. (2014) *The Biochemical journal* 457, 415-424.

60. Ujjainwalla, F. & Walsh, T. F. (2001) *Tetrahedron Lett* 42, 6441-6445.

61. Polucci, P., Magnaghi, P., Angiolini, M., Asa, D., Avanzi, N., Badari, A., Bertrand, J., Casale, E., Cauteruccio, S., Cirla, A*., et al.* (2013) *Journal of medicinal chemistry* 56, 437-450.

62. Hur, W., Sun, Z., Jiang, T., Mason, D. E., Peters, E. C., Zhang, D. D., Luesch, H., Schultz, P. G., & Gray, N. S. (2010) *Chemistry & biology* 17, 537-547.

63. Eggler, A. L., Luo, Y., van Breemen, R. B., & Mesecar, A. D. (2007) *Chemical research in toxicology* 20, 1878-1884.

64. Fourquet, S., Guerois, R., Biard, D., & Toledano, M. B. (2010) *The Journal of biological chemistry* 285, 8463-8471.

65. Linker, R. A., Lee, D. H., Ryan, S., van Dam, A. M., Conrad, R., Bista, P., Zeng, W., Hronowsky, X., Buko, A., Chollate, S*., et al.* (2011) *Brain* 134, 678-692.

66. Cleasby, A., Yon, J., Day, P. J., Richardson, C., Tickle, I. J., Williams, P. A., Callahan, J. F., Carr, R., Concha, N., Kerns, J. K*., et al.* (2014) *PloS one* 9, e98896.

67. Weerapana, E., Wang, C., Simon, G. M., Richter, F., Khare, S., Dillon, M. B., Bachovchin, D. A., Mowen, K., Baker, D., & Cravatt, B. F. (2010) *Nature* 468, 790-795.

68. Qian, Y., Martell, J., Pace, N. J., Ballard, T. E., Johnson, D. S., & Weerapana, E. (2013) *Chembiochem* 14, 1410-1414.

69. Eng, J. K., McCormack, A. L., & Yates, J. R. (1994) *Journal of the American Society for Mass Spectrometry* 5, 976-989.

70. Tabb, D. L., McDonald, W. H., & Yates, J. R., 3rd (2002) *Journal of proteome research* 1, 21-26.

71. Weerapana, E., Speers, A. E., & Cravatt, B. F. (2007) *Nat Protoc* 2, 1414-1425.

72. Baird, L., Swift, S., Lleres, D., & Dinkova-Kostova, A. T. (2014) *Biotechnology advances* 32, 1133-1144.

73. Bertrand, H. C., Schaap, M., Baird, L., Georgakopoulos, N. D., Fowkes, A., Thiollier, C., Kachi, H., Dinkova-Kostova, A. T., & Wells, G. (2015) *Journal of medicinal chemistry* 58, 7186-7194.

74. Jung, K. A. & Kwak, M. K. (2010) *Molecules* 15, 7266-7291.

75. Innamorato, N. G., Rojo, A. I., Garcia-Yague, A. J., Yamamoto, M., de Ceballos, M. L., & Cuadrado, A. (2008) *J Immunol* 181, 680-689.

76. Koh, K., Kim, J., Jang, Y. J., Yoon, K., Cha, Y., Lee, H. J., & Kim, J. (2011) *Journal of neuroimmunology* 233, 160-167.

77. Hornung, V., Bauernfeind, F., Halle, A., Samstad, E. O., Kono, H., Rock, K. L., Fitzgerald, K. A., & Latz, E. (2008) *Nature immunology* 9, 847-856.

78. Trager, U., Magnusson, A., Lahiri Swales, N., Wild, E., North, J., Lowdell, M., & Bjorkqvist, M. (2013) *PLoS currents* 5.

79. Slow, E. J., van Raamsdonk, J., Rogers, D., Coleman, S. H., Graham, R. K., Deng, Y., Oh, R., Bissada, N., Hossain, S. M., Yang, Y. Z*., et al.* (2003) *Human molecular genetics* 12, 1555-1567.

80. Kwan, W., Magnusson, A., Chou, A., Adame, A., Carson, M. J., Kohsaka, S., Masliah, E., Moller, T., Ransohoff, R., Tabrizi, S. J*., et al.* (2012) *J Neurosci* 32, 133-142.

81. Mangiarini, L., Sathasivam, K., Seller, M., Cozens, B., Harper, A., Hetherington, C., Lawton, M., Trottier, Y., Lehrach, H., Davies, S. W*., et al.* (1996) *Cell* 87, 493-506.

82. Ritch, J. J., Valencia, A., Alexander, J., Sapp, E., Gatune, L., Sangrey, G. R., Sinha, S., Scherber, C. M., Zeitlin, S., Sadri-Vakili, G*., et al.* (2012) *Molecular and cellular neurosciences* 50, 70-81.

83. An, M. C., Zhang, N., Scott, G., Montoro, D., Wittkop, T., Mooney, S., Melov, S., & Ellerby, L. M. (2012) *Cell Stem Cell* 11, 253-263.

84. Lee, O. H., Jain, A. K., Papusha, V., & Jaiswal, A. K. (2007) *The Journal of biological chemistry* 282, 36412-36420.

85. Crotti, A., Benner, C., Kerman, B. E., Gosselin, D., Lagier-Tourenne, C., Zuccato, C., Cattaneo, E., Gage, F. H., Cleveland, D. W., & Glass, C. K. (2014) *Nat Neurosci* 17, 513-521.

86. Lastres-Becker, I., Innamorato, N. G., Jaworski, T., Rabano, A., Kugler, S., Van Leuven, F., & Cuadrado, A. (2014) *Brain* 137, 78-91.

87. (2012) *Cell Stem Cell* 11, 264-278.

88. Ernst, A., Alkass, K., Bernard, S., Salehpour, M., Perl, S., Tisdale, J., Possnert, G., Druid, H., & Frisen, J. (2014) *Cell* 156, 1072-1083.

89. Jin, Y. N., Yu, Y. V., Gundemir, S., Jo, C., Cui, M., Tieu, K., & Johnson, G. V. (2013) *PloS one* 8, e57932.

90. Xu, K., Xu, Y., Brown-Jermyn, D., Chen, J. F., Ascherio, A., Dluzen, D. E., & Schwarzschild, M. A. (2006) *J Neurosci* 26, 535-541.

91. Chen, X., Burdett, T. C., Desjardins, C. A., Logan, R., Cipriani, S., Xu, Y., & Schwarzschild, M. A. (2013) *Proceedings of the National Academy of Sciences of the United States of America* 110, 300-305.

92. Ehrlich, M. E., Conti, L., Toselli, M., Taglietti, L., Fiorillo, E., Taglietti, V., Ivkovic, S., Guinea, B., Tranberg, A., Sipione, S.*, et al.* (2001) *Exp Neurol* 167, 215-226.

93. Quinti, L., Chopra, V., Rotili, D., Valente, S., Amore, A., Franci, G., Meade, S., Valenza, M., Altucci, L., Maxwell, M. M.*, et al.* (2010) *PLoS currents* 2.

94. Lleres, D., James, J., Swift, S., Norman, D. G., & Lamond, A. I. (2009) *The Journal of cell biology* 187, 481-496.

95. Marder, K., Zhao, H., Myers, R. H., Cudkowicz, M., Kayson, E., Kieburtz, K., Orme, C., Paulsen, J., Penney, J. B., Jr., Siemers, E.*, et al.* (2000) *Neurology* 54, 452-458.

96. Chopra, V., Quinti, L., Kim, J., Vollor, L., Narayanan, K. L., Edgerly, C., Cipicchio, P. M., Lauver, M. A., Choi, S. H., Silverman, R. B.*, et al.* (2012) *Cell reports* 2, 1492-1497.

97. Chen, X., Wales, P., Quinti, L., Zuo, F., Moniot, S., Herisson, F., Rauf, N. A., Wang, H., Silverman, R. B., Ayata, C.*, et al.* (2015) *PloS one* 10, e0116919.

98. Zhang, B. R., Tian, J., Yan, Y. P., Yin, X. Z., Zhao, G. H., Wu, Z. Y., Gu, W. H., Xia, K., & Tang, B. S. (2012) *J Neurol Sci* 312, 92-96.

Figure Legends

Fig. 1. MIND4 is neuroprotective in MPTP-toxicity mouse model. **A)** Brain-permeability of MIND4, administered by intraperitoneal (i.p.) injections to wild type mice. Chromatograms of

MIND4 standard (1µg/ml) and MIND4-treated brain are shown. HPLC analysis detected MIND4 at 0.45 µg/ml concentration in mouse cortical extracts, providing preliminary evidence for compound brain permeability. **B**) MIND4 effective dose was established in mice using subacute MPTP treatment paradigm: MPTP untreated control (CTR) and MPTP treated mice with administered by i.p. vehicle alone or with MIND4 at 30 and 60 mg/kg dose. Vehicle or MIND4 were administered 10 min before and 50 min after each MPTP injection. Levels of dopamine (DA) were determined by HPLC-ECD. Statistical significant increase of DA was observed in mice treated with MIND4 at 60mg/kg. n=5-8 * = $p < 0.05$; ** = $p < 0.01$. **C**) MIND4 at 60mg/kg before and after administration of 20mg/kg MPTP does not change metabolism of neurotoxin in the striatum. MPP^+ was examined by HPLC 90 min after the second MIND4 administration. **D-G**) Degeneration of dopaminerigic neurons was induced in mice using subacute MPTP-treatment paradigm (20mg/kg *i.p.* injection once daily for 4 days) and MIND4 administered by i.p. at established effective dose 60mg/kg) 10 min before and 50 min after each MPTP injection. **D, E**) MIND4 attenuated MPTP induced dopamine (DA) depletion (**D**) and high DA turnover rate (**E**) (n=5-8). **F**) Stereological quantification of TH neurons (n=5-8). (* = $p < 0.05$; ** = $p < 0.01$; *** = $p < 0.001$). **G**) MIND4 treatment preserves SN dopaminergic neurons in MPTP mice. **H-K**) Analysis of pharmacodynamic markers in stiatal samples (**D-G**): NRF2 activation (increase GCLM levels) and SIRT2 inhibition (increase α-tubulin acetylation) in MPTP-challenged brains from MIND4-treated and untreated mice . Levels of GCLM (**H**) and acetylated α-tubulin (**I**) and α-tubulin (loading control) were detected by immunoblotting. **J**) Densitometry analysis of (**H**). Mean of GCLM signal is statistically significantly greater in MIND4-tretaed then in untreated samples (n=5). * = $p < 0.5$. **K**) Densitometry analysis of (**I**). Mean of acetylated α-tubulin shows no statistically significant difference in cohorts of MIND4-treated vs untreated cohorts. Levels of total α-tubuin were used for normalization in (**J**) and (**K**).

Fig. 2. Characterization of NRF2 inducer MIND4-17. **A)** Structure of parent MIND4 and lead-inducer MIND4-17. **B)** Concentration-dependent activity test of MIND4-17, structural analogs MIND4-17-15, MIND4, MIND4B, and control NRF2 inducers SFP and DMF in quantitative NQO1 inducer bioassay. The standard deviation in each data point (n=8) < 5%. **C-F, H)** Levels of NRF2 and NRF2-responsive NQO1 and GCLM proteins and GADPH, β-actin, LAMIN used as loading control were detected by immunoblotting. **C)** Induction of NRF2-responsive NQO1 and GCLM proteins in MIND4 and DMF treated mutant HD ST14A cells. **D)** Compound activity test shows no induction of NQO1 in NRF2-KO MEFs treated with MIND4-17 and its analogs. Induced NQO1 level in wild-type MEFs is shown for comparison. **E)** Concentration-dependent stabilization of NRF2 protein in wild-type MEFs treated with MIND4-17, MIND4, MIND4B, or SFP. **F)** Time-dependent accumulation of NRF2 in cytoplasmic and nuclear fractions from wild-type MEFs treated MIND4-17. Cell lysis and biochemical fractionation were performed at the indicated treatment times. **G)** MIND4-17 covalently modifies a single cysteine -151 in the BTB domain of KEAP1. Overlay of the deconvoluted intact protein mass spectra obtained from BTB [48-190/S182A] (theoretical mass 16175.6 Da) in buffer (red) vs. treated with MIND4-17 (blue). **H)** MIND4-17 treatment stabilizes NRF2 in COS1 cells co-expressing NRF2-V5 and KEAP1 wild-type or double-mutant C226S/C613S KEAP1 but not a single mutant C151S.

Fig. 3. MIND4-17 arrests KEAP:NRF2 complex in the *closed* conformation in live cells. **A)** Fluorescence lifetime imaging of cells co-expressing either EGFP-NRF2 + free mCherry or EGFP-NRF2 + KEAP1-mCherry, and treated with vehicle (DMSO) or MIND4-17 (1 μM) for 1 h. HEK293 cells were transfected with the indicated constructs, and the fluorescence lifetime of EGFP and the FRET efficiency quantified in the cytoplasm 24 h later. The first column shows the EGFP intensity images from which the lifetime data were derived, while the second column shows mCherry intensity images. The third column depicts EGFP fluorescence lifetime where pixel color corresponds to the mean lifetime of EGFP, ranging from 1.9 to 2.5 ns as indicated in

the color-scale below each image. The fourth column shows the lifetime data histograms for each image, with lifetime on the x-axis and pixel frequency on the y-axis. **B)** Quantification of the *open* and *closed* conformations of the KEAP1:NRF2 protein complex based on the FRET efficiency distribution across the cytoplasm. The sub-population of FRET efficiency between 0-15% was assigned the "*open*" conformation of the complex, while the FRET population between 15-30% the "*closed*" conformation of the complex. Data represent means ± SD from 6 to 17 cells.
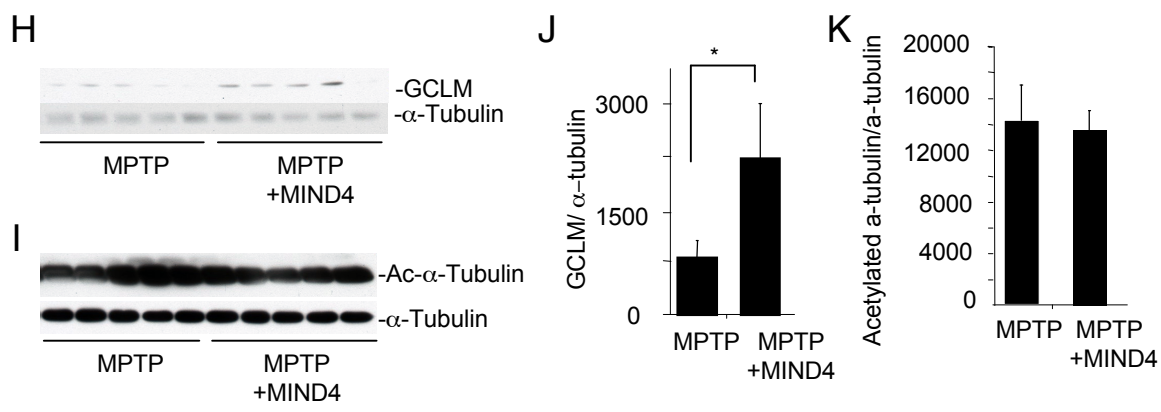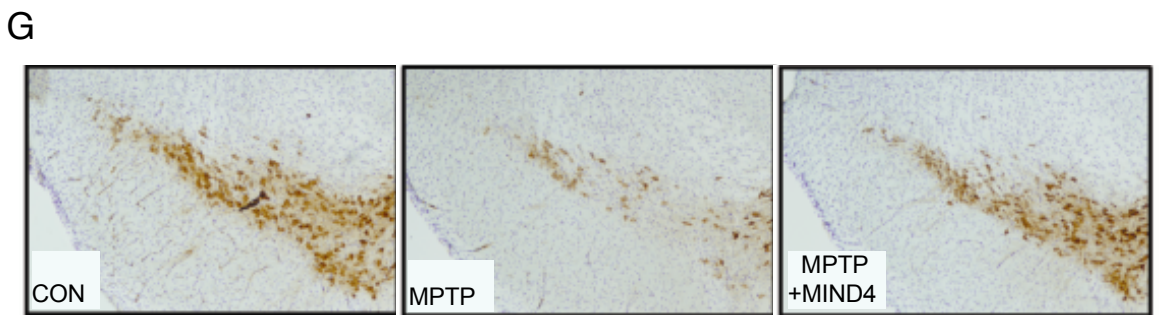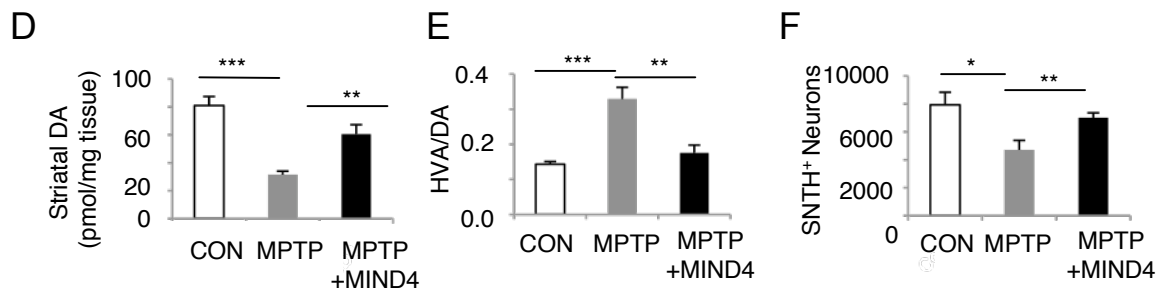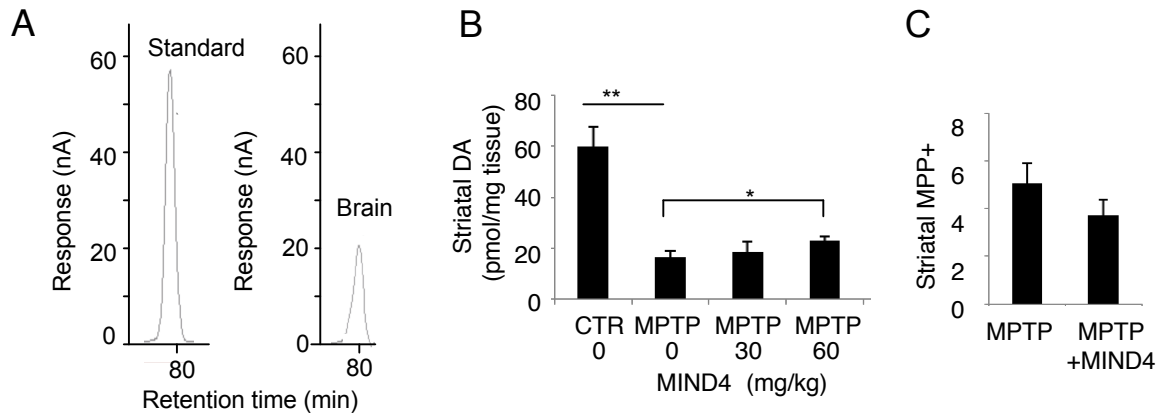
Fig 4. NRF2 activation by MIND4-17 has anti-inflammatory effects in mouse microglia cells. **A-F)** Evaluation of NRF2-specific transcriptional responses in resting and LPS-activated BV2 microglial cells treated with MIND4-17. Concentration-dependent effects of MIND4-17 treatment on mRNA expression of NRF2-responsive anti-oxidant *GCLM* (**A**) and *NQO1* (**B**), and pro-inflammatory cytokine *Il-6* (**C**), *IL-1β* (**D**), *TNF*a (**E**), and *MCP-1* (**F**) genes. Transcriptional expression was measured using qRT-PCR with gene-specific primers in duplicates (n=2). Means (filled bars) and standard error bars are shown. **G-H)** MIND4-17 concentration-dependent effects on secretion of IL6 in primary microglia (**G**) and astrocytes (**H**) from wild-type (WT) and HD (YAC 128); inflammatory responses were induced with CSE and INF-γ. Combined graphs of two independent experiments are shown. Filled circles (WT) and open squares (YAC128) represent mean values (n=2) from compound-treated cells expressed as a percent from vehicle (DMSO)-treated cells (100%), standard error bars are shown.

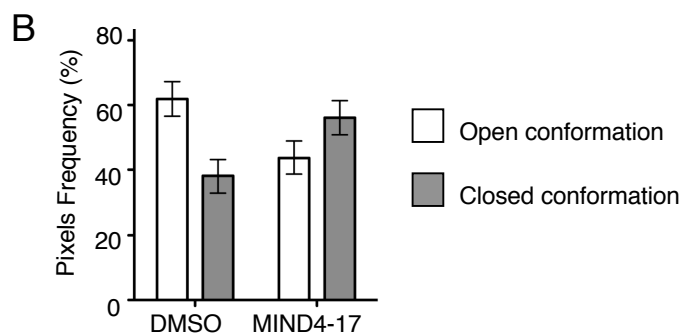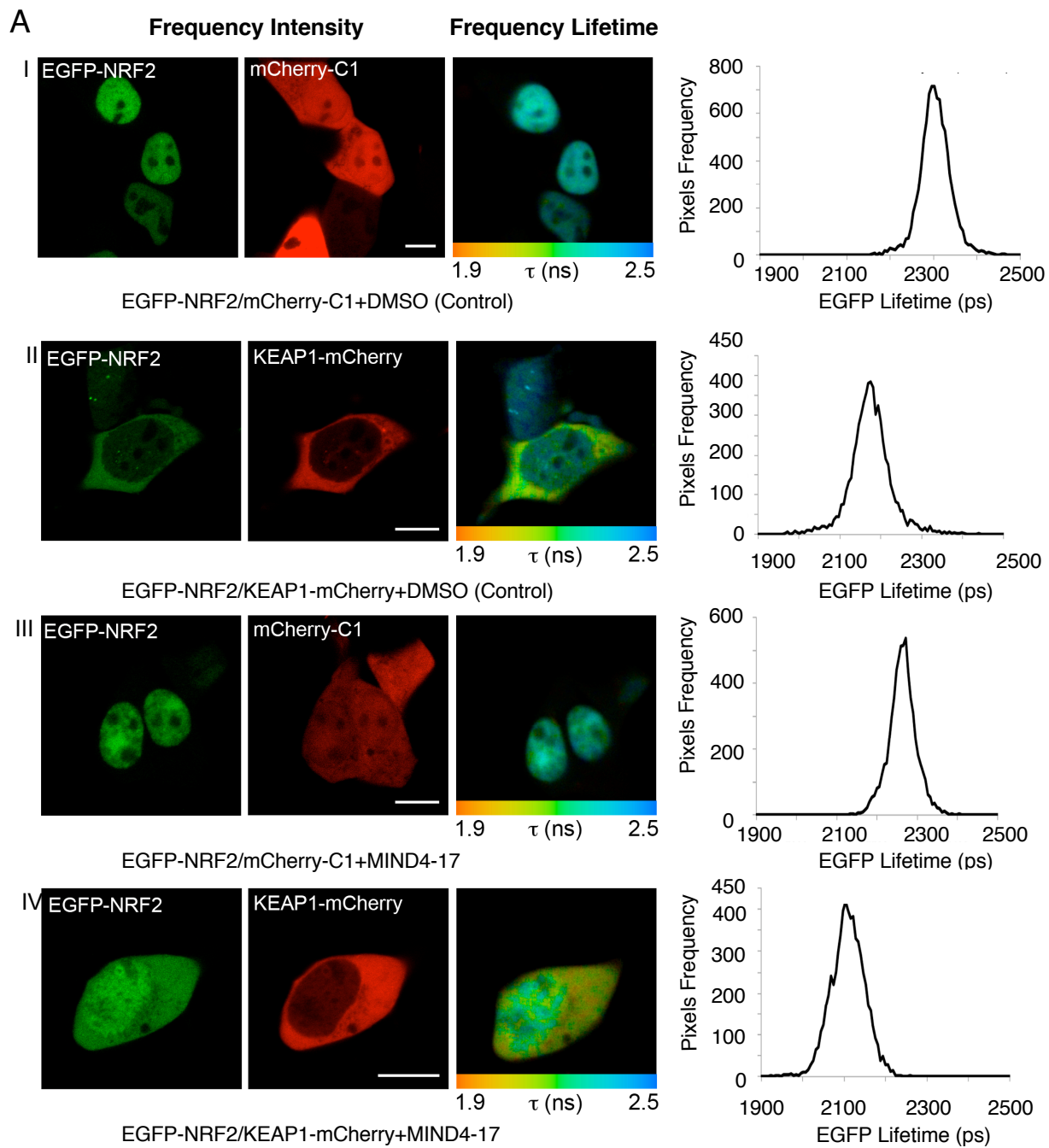NRF2 activation by MIND4-17 has anti-inflammatory effects in mouse microglia cells

Fig. 5. Characterization of anti-inflammatory NRF2-dependent responses in primary human monocytes treated with MIND4-17. **A-H)** MIND4-17 represses expression of induced inflammatory cytokines in primary monocytes from normal subjects (**A-D**) and HD patients (**E-H**). IL-1b, IL-6, IL-8, and TNFα, production by LPS and IFN-γ stimulated monocytes, measured by multiplex ELISA, was compared in cells treated with different concentrations of MIND4-17

and with similar doses of vehicle (DMSO). Linear mixed model on log transformed data, n= 10 controls, n= 13 for HD patients, +/- SEM, * = p<0.05; ** = p<0.01, *** = p<0.001. (One-Way ANOVA p=0.61, n= 13).
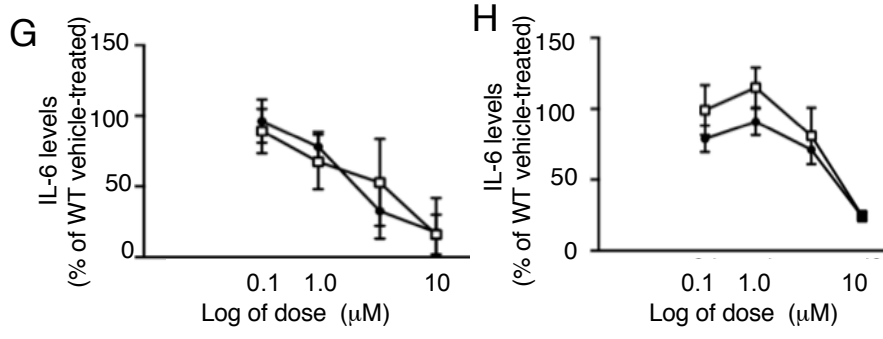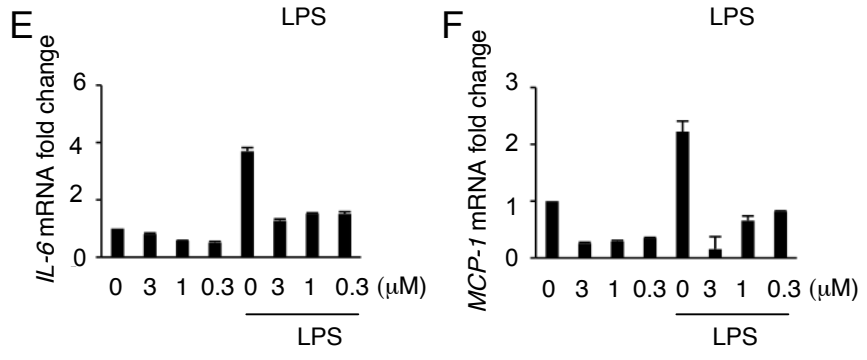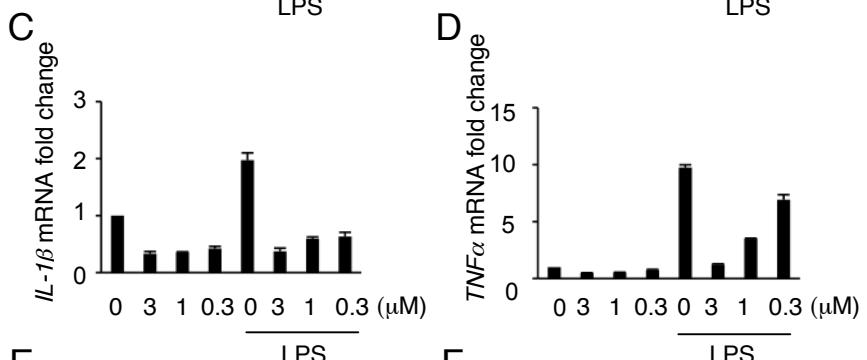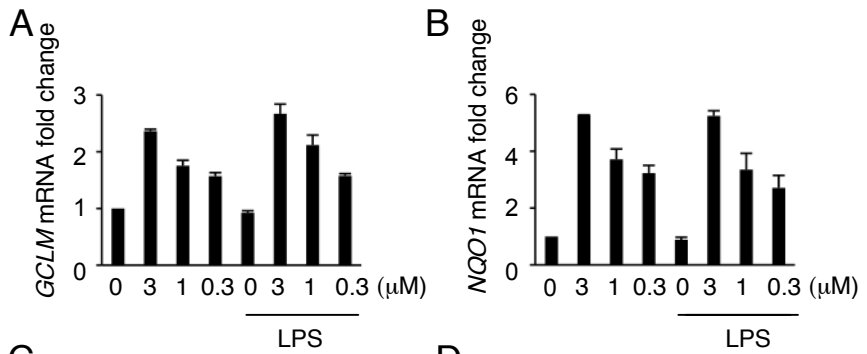
Fig. 6. Activation of NRF2 signaling in human iPSC-derived neural stem cells. **A)** MIND4-17 induces NQO1 and GCLM protein expression in HD48, HD51 and WT54, WT55 NSCs. Cells were treated with MIND4-17 for 24 h at indicated concentrations. Protein levels were detected by immunoblotting. **B)** No effects of MIND4-17 treatment on mutant or wild-type HTT levels in HD51 and WT55 NSCs in were detected. **C)** HD48 and HD51 extracts from (**A**) were diluted 1:3 and NQO1 levels re-examined. **D)** Densitometric analysis of NQO1 expression in HD48 and HD51 (black bars) and WT54 (grey bars) NSCs. Data are presented as mean ± SD of two independent experiments. *p <0.05 by t-test; n=4. **E)** Relative induction of NQO1 expression in WT54 (grey triangle/line) and HD51 (black triangle/line) NSCs treated with MIND4-17 at indicated concentrations. Each data point represents a mean ± SD of two independent experiments; n=4. **F-I)** Effects of MIND4-17 in mutant HD4 and in genetically corrected isogenic non-disease HD116c. **F)** Basal levels of NQO1, GCLM, and a-tubulin in HD4 and HD116c, detected by immunoblotting. **G, H)** MIND4-17 induces expression of NQO1 and GCLM in the corrected HD116c (**H**) but not in the parental HD4 (**G**) cell lines. NQO1 and GCLM protein expression levels and α–tubulin were detected by immunoblotting. **I-J)** Densitometric analysis of NQO1 (**I**) and GCLM (**J**) induction in HD4 from (**G**) shows no induction of NRF2-responsive proteins by MIND4-17. Levels of α-tubulin served as the loading control and were used for normalization of NQO1 or GCLM signals. **K)** Densitometric analysis of NQO1 induction in HD116c. Signals were normalized to the levels of α-tubulin. Data are presented as means ± SD; t-test with Holm correction for multiple comparison. ***p <0.01; n=4.

A

Standard

Brain

Response (nA)

Retention time (min)

B

Striatal DA (pmol/mg tissue)

**

*

CTR   MPTP   MPTP   MPTP
0   0   30   60
MIND4 (mg/kg)

C

Striatal MPP+

MPTP   MPTP
+MIND4

D

Striatal DA (pmol/mg tissue)

***

**

CON   MPTP   MPTP
+MIND4

E

HVA/DA

***   **

CON   MPTP   MPTP
+MIND4

F

SNTH+ Neurons

*   **

CON   MPTP   MPTP
+MIND4

G

CON

MPTP

MPTP
+MIND4

H

-GCLM
-α-Tubulin

MPTP   MPTP
+MIND4

I

-Ac-α-Tubulin
-α-Tubulin

MPTP   MPTP
+MIND4

J

GCLM/ α–tubulin

*

MPTP   MPTP
+MIND4

K

Acetylated a-tubulin/a-tubulin

MPTP   MPTP
+MIND4

A

MIND4   MIND4-17

B

NQO1 Specific Activity Treated/Control

- MIND4
- MIND4-17
- MIND4-17-15
- MIND4B
- DMF
- SFP

(μM)

C

HD MUTANT

-NQO1
-GCLM
-GAPDH

0   1   2   5   10   .1   .5   1   (μM)

DMF   MIND4-17

D

NRF2 KO MEF   WT

-NQO1
-β-actin

0   1.25   2.5   5   1.25   2.5   5   0.125   0.25   0.5   0.125   0.25   0.5   5   (μM)

MIND4   MIND4B   MIND4-17   MIND4-17-15   MIND4

E

-NRF2
-β-actin

0   1.25   2.5   5   1.25   2.5   5   0.125   0.25   0.5   1.25   2.5   3.0   0   (μM)

MIND4   MIND4B   MIND4-17   SFP

F

Cytosolic   Nuclear   Fraction

-NRF2
-GAPDH
-Lamin A/C

0   30   60   180   300   0   30   60   180   300   -minutes

G

Intensity (counts)

16175.6   16298.0

ΔMass = 122.4 Da

Mass (Da)

H

WT   C151S   C226S/C613S   WT   WT   C151S   C151S   C226S/C613S   C226S/C613S

170kD—
100kD—   -NRF2 (V5)
                -KEAP1

Vehicle   MIND4-17 (5μM)

A

Frequency Intensity | Frequency Lifetime

I EGFP-NRF2 | mCherry-C1
1.9 τ (ns) 2.5
EGFP-NRF2/mCherry-C1+DMSO (Control)

II EGFP-NRF2 | KEAP1-mCherry
1.9 τ (ns) 2.5
EGFP-NRF2/KEAP1-mCherry+DMSO (Control)

III EGFP-NRF2 | mCherry-C1
1.9 τ (ns) 2.5
EGFP-NRF2/mCherry-C1+MIND4-17

IV EGFP-NRF2 | KEAP1-mCherry
1.9 τ (ns) 2.5
EGFP-NRF2/KEAP1-mCherry+MIND4-17

B

Open conformation
Closed conformation

DMSO   MIND4-17

Materials and Methods

Formulation, tolerability, and pharmacokinetics of MIND4

MIND4 was solubilized at 5mg/ml in 7.5% Cremophor EL (BASF)/2.375% Ethanol in PBS.

Wild-type mice C57BL/6 (n=3) were subjected to compound treatment at escalated dosing from

50 mg/kg up to a final dose of 275 mg/kg administered daily by intraperitoneal (i.p.) injection. No

weight loss or sudden death were observed suggesting lack of acute toxicity of MIND4 in that

dose range. Mice were sacrificed 2 h following the last drug administration and cortical samples

isolated according to standard procedure and subjected to HPLC analysis as described (96, 97).

Pharmacokinetics was performed in male C57BL/6 mice (n=3) at 0.5, 1.0, 2, 4, 8, and 24 h post

i.p. injection of MIND4 at 50 mg/kg and collected serum samples analyzed by HPLC. Mice (n=3)

were sacrificed at 0.5 h post i.p. injection of MIND4 at 50 mg/kg dose and isolated cortical

samples were subjected to HPLC analysis.

Quantification of MIND4 using HPLC-EC: Frozen mouse cortical tissues were extracted in ice-

cold methanol containing 0.4% acetic acid (approximately 1:6 ratios), probe sonicated for 5 sec

and centrifuged at 22.000 g for 20 min at 4^0 C. The supernatant was dried under centrifugation

and vacuum and reconstituted with running buffer. Reverse phase- HPLC/ECA separation was

accomplished on Shiseido MG240 C18 HPLC column (4.6x250 mm, 3 μ particle size), flow rate

1ml/min, using 50% methanol in 0.1M sodium phosphate buffer pH 3, isocratic elution was

performed for 20 min using 4 channel electrochemical array. Levels of MIND4 were determined

using integrated peak areas and the standard probe.

Analysis of TNFa levels in cortex of MIND4-terated R6/2 mice

Female R6/2 mice used in the study were generated by back-crossing R6/2 males from

The Jackson Laboratory, Bar Harbor, ME with C57BL/6 X CBA F1 females and maintained at MGH animal facility. Mice were genotyped by PCR using tail-tip DNA and were housed five per cage under standard conditions with *ad libitum* access to water and food. Mice were administered with MIND4 at the dose of 50 mg/kg by i.p. injections for 2 weeks. The drug suspension at 5mg/ml in 7.5% Cremophor EL (BASF)/2.375% Ethanol in PBS, was made fresh daily. At 10 weeks of age, R62 and age-matching wild type control mice were sacrificed 2 h after last injections, brains were removed and snap frozen in liquid nitrogen and kept frozen at -80^0 C until analyzed. All animal experiments were carried out in accordance with the National Institutes of Health Guide for the Care and Use of Laboratory Animals and were approved by local animal care committee.

SIRT2 deacetylase activity test

Deacetylation reaction was performed at 37^0C for 1hr in the presence of human recombinant enzymes: SIRT2 (BioMol-SE-251) 5 units/per reaction, compound of interest, standard buffer, $50\mu M$ substrate, and $500\mu M$ NAD$^+$ according to manufacturer protocol and as described previously (55).

Compound activity test in the rat embryonic striatal cell lines ST14A

ST14A cells (a generous gift of E. Cattaneo) (92) stably express either a mutant expanded repeat (128Q) or wild-type (26Q) 546 amino acid huntingtin (HTT) fragment and were treated with compounds for 24 h as described (93). Protein levels of NQO1, GCLM, and α-tubulin (loading control) were detected in ST14A by immunoblotting with NQO1 (Sigma, 1:1,000), GCLM (Abcam, 1:800), and GAPDH (Millipore, 1:10,000) antibodies.

Nuclear-cytoplasmic extract separation

Nuclear WT MEFs (500,000 per dish) were grown for 24 h on 6 cm plates, and then treated with

solvent control (0.1% DMSO, v/v) or 0.5 μM MIND4-17. At the end of each treatment time, cells were washed twice in PBS and lysed in buffer A [10 mM KCl, 5 mM MgCl₂, 50 mM Tris-HCl (pH 7.5), 0.5% NP-40, 1 mM DTT], containing 1 protease inhibitor and 1 phosphatase inhibitor tablets (Roche) per 10 mL buffer. Lysates were subjected to centrifugation at 1,000 x g for 5 min at 4°C and supernatant (cytoplasmic fraction) was transferred to a fresh microfuge tube. The pellet (nuclear fraction) was washed three times in buffer A before being dissolved in buffer B [2% SDS, 150 mM NaCl, 65 mM Tris-HCl (pH 8.0)] and sonicated for 30 sec. Finally, the lysates were subjected to Western blot analysis with NRF2 antibody and with GAPDH (rabbit polyclonal, 1:5000) and lamin A/C (rabbit polyclonal, 1:1000, Gene Tex) to confirm fraction purity and equal protein loading.

Design and synthesis of MIND4-17 analogs

MIND4-17 analogs 2286, 2291 and 2907 were synthesized as shown in Scheme 1 (**Fig. S3**). Compound A was prepared following a previously reported method (61). Compound A was converted to 2291, 2907 and MIND4-17 by reacting with 4-nitroflurobenzene, 2-chloro-5-nitropyridine and 2-chloropyridine respectively. The nitro group in MIND4-17 was then reduced with stannous chloride to give 2286. 2909 was synthesized as shown in Scheme 2 (**Fig. S3**). Compound B was synthesized by coupling 2-chloro-5-nitropyridine and *tert*-butyl methyl malonate (60). Treatment of Compound B with hydrazine gave compound C, which upon reaction with 3-phenoxy acetyl chloride gave compound D. 2909 was obtained by reacting compound D with aniline and phosphorous trichloride. 2872 was prepared as shown in Scheme 3 (**Fig. S3**). Compound E was obtained by reacting phenol with ethyl bromoacetate under basic conditions. The ester group in compound E was converted the hydrazide F by reacting with hydrazine. Compound F was reacted with phenylisocyanate and cyclized under basic condition to yield compound H, which was reacted with 2-chloro-5-nitropyridine to give 2872. Synthesis of MIND4-17 and respective analogs was conducted by a drug discovery company Aurigene (co-

authors V.P. and S. S); NMR analysis shows an acceptable 95% purity. The activities of MIND4-17, synthesized by Aurigene, and commercially purchased from Cambridge (multiple batches) were identical and activities of analogs consistent with established mechanism.

Compound GSH sensitivity assay.

Hepa1c1c7 cells. Each compound was incubated in cell culture medium in the presence or absence of 1mM GSH at 37ºC for 30 min before administering to Hepa1c1c7 cells grown on 96-well plates. After a 48 h exposure, the NQO1 enzyme activity was determined in cell lysates. Results are shown as average values of 8 replicate wells. The standard deviation in each case was less than 5%.

Fluorescence lifetime imaging analysis of MIND4-17effect on NRF2 : KEAP1 complex

Fluorescence lifetime imaging microscopy (FLIM) was performed as described (Llères et al , 2009) using an inverted multiphoton laser-scanning microscope (Zeiss LSM780 Confocal) with a 63x oil immersion NA 1.4 Plan-Apochromat objective from Zeiss. The software used to run the LSM780 multiphoton microscope was Zen 2010. The microscope was equipped with a black incubation chamber suitable to maintain the live cells and optics at constant temperature 37 °C. Two-photon excitation of EGFP was achieved using a Coherent Scientific Chameleon Ultra II Ti:Sapphire laser (tuning range 680-1080 nm) at 890 nm. The fluorescence lifetime imaging capability was provided by time-correlated single photon-counting (TCSPC) electronics (SPC-830; Becker & Hickl GmbH). Laser power was adjusted to give a mean photon count rate of the order 10^4–10^5 photons/s. Fluorescence lifetime measurements were acquired over 90 s. Fluorescence lifetimes were calculated for all pixels in the field of view (256 × 256 pixels) and then a particular region of interest (e.g., cytoplasm) was selected using SPCImage software (Becker & Hickl GmbH). The analysis of the FLIM measurements from a particular region of interest was performed by using SPCImage software. The best-fitting model (k^2 of the fit close to

one) to extract an accurate fluorescence lifetime value from the decays was applied by adjusting several parameters such as the number of exponential components, the background threshold, the shift index and the scatter parameter (amount of scattered excitation light detected).

The FRET efficiency percentage was calculated using SPCImage software for the same region defined to calculate the mean fluorescence lifetime. The image was then analyzed using a two-component exponential decay model were the lifetime t2 (non-interacting proteins lifetime from EGFP-NRF2 +free mCherry cells) was fixed, whereas the t1 value (lifetime associated to the donor proteins interacting with the acceptor) was left unchecked. Pixel enrichment in the respective FRET populations related to *open* (0-15%) or *closed* (15-30%) conformation was quantified from the lifetime distribution histograms. The lifetime histogram for each vehicle and MIND4-17 treated cells was normalized by the total number of pixels $Fi = fi/Ni$, where fi and Ni are the lifetime histogram and the total number of pixels, respectively.

Mass spectrometry analysis of KEAP1 BTB modification by MIND4-17

The BTB domain of Keap1 (residue 48-190) was cloned into a modified pET19 vector with N-terminal 6xHis-tag cleavable with TEV protease and a single point mutation was introduced at position 182 (S182A). The full length KEAP1 with deletion of the first 54 amino acids was cloned in similarly in the same expression vector. The overexpression and purification were performed as described in (66).

For analysis of the potential modification of the BTB domain, 10 µM BTB [48-190 S182A] were incubated with 2mM MIND4-17 (or DMSO 2% final concentration for control) for an hour on ice in 20 mM TrisHCl pH 8.0, 150 mM NaCl. Intact protein masses were determined through HPLC-coupled ESI-MS on an AB Sciex TripleTOF 5600+ mass spectrometer (Sciex, Darmstadt, Germany). Intact protein were first concentrated and washed on a Piccolo Proto 200 C4 5µm 2.5 x 0.5mm trap column (Higgins Analytical, Mountain View, CA) and subsequently switched in line with, and separated on, a Jupiter C4 5µm 300Å 150 x 1 mm analytical column (Phenomenex,

Torrance, CA) mounted onto a Shimadzu Prominence UFLC (Shimadzu, Duisburg, Germany) at a 70μl min^{-1} flow rate with the following buffers: A – 5% ACN, 5% DMSO, and 0.1% FA; B – 90% ACN, 5% DMSO, and 0.1% FA. Proteins were then eluted over with a gradient of 3 minutes of 1% B to 55% B followed by 1 minute of 55% B to 90% B. Mass analysis was performed by ESI-TOF-MS on an AB Sciex TripleTOF 5600+ mass spectrometer (Sciex, Darmstadt, Germany) with a DuoSpray Ion Source with the following settings: floating voltage of 5500V, temperature of 350°C, declustering potential of 120 with 4 separate TOF experiments each respectively with 4, 12, 20 and 40 time bins summed. Data analysis was performed as follows: spectra were integrated over a retention time period, and the summed TOF experiment with the greatest resolution selected. The raw data was then converted and deconvoluted using the MaxEnt I algorithm (Waters, Milford, MA) at a resolution of 0.1 Da.

Proteomic analysis by quantitative Mass-Spectrometry

Preparation of mass-spectrometry samples for reactive cysteine profiling: HeLa soluble protein lysates (500 uL, 2 mg mL-1) were aliquoted, and MIND4-17 (10 μM), or DMSO was added to the appropriate samples at the designated concentration. Two aliquots were made for each inhibitor concentration or DMSO equaling 4 tubes for one final sample. The samples were incubated at RT for 1 h. IA-alkyne (100 μM) was added to the samples and incubated at RT for 1 hr. Inhibitor treated and DMSO samples were functionalized with Azo-H tag or Azo-L tag (100 μM, 50X stock in DMSO) respectively (68). All samples were then treated with TCEP (1 mM, 50X fresh stock in water), TBTA ligand (100 μM, 17X stock in DMSO:*t*-butanol = 1:4), and copper(II) sulfate (1 mM, 50X stock in water) followed by incubation at RT for 1 hr. Samples were combined pairwise to combine inhibitor and DMSO-treated samples and centrifuged (6500 g, 4 min, 4 °C) to pellet the precipitated proteins. The pellets were resuspended in cold methanol by sonication and the two samples were combined. Centrifugation was followed by a second methanol wash, after which the pellet was solubilized in DPBS containing 1.2% SDS via

sonication and heating (90 °C, 5 min). The 2 samples resulting from inhibitor pretreatment, IA-alkyne incubation, and Azo-H or Azo-L labeling are as follows: Heavy (DMSO, 100 μM IA-Alkyne)/light (10 μM MIND4-17, 100 μM IA-Alkyne).

The SDS-solubilized proteome samples were diluted by 5 mL of DPBS for a final SDS concentration of 0.2%. The solution was incubated with 100 μL of streptavidin-agarose beads (Thermo Scientific, washed 3X with DPBS to remove storage buffer) overnight at 4 °C. Samples were rotated at RT for 2 h before washed by 5 mL 0.2 % SDS/DPBS, 3 X 5 mL DPBS, and 3 X 5 mL water. The beads were pelleted by centrifugation (1400 X g, 3 min) between washes.

The washed beads were suspended in 500 uL of 6 M urea/DPBS and 10 mM DTT (from 20X stock in water) and places in a 65 °C heat block for 15 min. Iodoacetamide (20 mM from 50X stock in water) was then added and the samples were allowed to react at 37 °C for 30 min. Following reduction and alkylation, the beads were pelleted by centrifugation and resuspended in 200 μL of 2 M urea/DPBS, 1 mM $CaCl_2$ (100X stock in water), and trypsin (2 μg). The digestion was allowed to proceed over night at 37 °C. The beads were pelleted by centrifugation and washed with 3 X 500 μL DPBS and 3 X 500 μL water. The azobenzene cleavage was carried out by incubating the beads with 50 μL of 25 mM sodium dithionite at RT for 1 h. The cleavage process was then repeated twice with 75 μL of 25 mM and 50 mM sodium dithionite and all the supernatants were combined. The beads were then washed twice with 75 μL of water and the wash was combined with the supernatant from the cleavage step to reach 350 μL final. Formic acid (17.5 μL) was added to the sample, which was stored at -20 °C until mass spectrometry analysis.

Quantitative mass-spectrometry analysis: LC/LC-MS/MS analysis was performed on an LTQ-Orbitrap Discovery mass spectrometer (ThermoFisher) coupled to an Agilent 1200 series HPLC. Peptide digests were pressure loaded onto a 250 μm fused silica desalting column packed with 4 cm of Aqua C18 reverse phase resin (Phenomenex). The peptides were eluted onto a biphasic column (100 μm fused silica with a 5 μ, tip, packed with 10 cm C 18 and 4 cm Partisphere strong

cation exchange resin (SCX, Whatman)) using a gradient 5-100% Buffer B in Buffer A (Buffer A: 95% water, 5% acetonitrile, 0.1% formic acid; Buffer B: 20% water, 80% acetonitrile, 0.1% formic acid). The peptides were then eluted from the SCX onto the C18 resin and into the mass spectrometer using 4 salt steps previously described (71). The flow rate through the column was set to ~0.25 μL/min and the spray voltage was set to 2.75 kV. One full MS scan (FTMS) (400-1800 MW) was followed by 8 data dependent scans (ITMS) of the nth most intense ions.

The tandem MS data were searched using the SEQUEST algorithm (69) using a concatenated target/decoy variant of the human IPI databases. A static modification of +57.02146 on cysteine was specified to account for alkylation by iodoacetamide and differential modifications of +462.2987 (IA-alkyne and cleaved Azo-H) and +456.2849 (IA-alkyne and cleaved Azo-L) were specified on cysteine to account for probe modifications. SEQUEST output files were filtered using DTASelect (70). Quantification of heavy/light ratios ($R_{H/L}$) was performed using the CIMAGE quantification package as previously described (67).

<u>Quantitative mass-spectrometry data for reactive-cysteine profiling upon MIND4-17 treatment:</u> Cysteine reactivity in proteomes pre-treated with MIND4-17 (Heavy-labeled) were compared to DMSO-treated samples (Light-labeled). For every cysteine-containing peptide, a heavy:light ratio was calculated that reflects the extent of cysteine reactivity in the inhibitor-treated versus DMSO samples. A ratio of 1 indicates that there was no change in cysteine reactivity, whereas ratio values >>1 show a loss in cysteine reactivity upon inhibitor treatment. Cysteine-containing peptides with ratio >2 for MIND4-17 are highlighted in green in **Dataset SI**, submitted as Excel spreadsheet.

Macrophages for drug testing experiment

Immortalized mouse bone marrow derived macrophages were a kind gift of Dr. Katherine Fitzgerald (UMASS Medical Center). Primary cells were immortalized by infection with J2 retrovirus as described (77). The LPS activation of macrophages, drug treatment, and

transcriptional profiling (**Fig. S3**) were conducted similar to experimental conditions described for microglia BV2 cells.

Compound transcriptional expression profiling microglia BV2 cells and macrophages

The following qPCR primers were selected using PrimerBank

(http://pga.mgh.harvard.edu/primerbank/) database:

mIL-1beta for 5'-GCAACTGTTCCTGAACTCAACT-3'

mIL-1beta rev 5'-ATCTTTTGGGGTCCGTCAACT-3'

mIL-6 for 5'-TAGTCCTTCCTACCCCAATTTCC-3'

mIL-6 rev 5'-TTGGTCCTTAGCCACTCCTTC-3'

mGAPDH for 5'-TGTGTCCGTCGTGGATCTGA-3'

mGAPDH rev 5'-GGTCCTCAGTGTAGCCCAAG-3'

mNQO1 for 5'-AGGATGGGAGGTACTCGAATC-3'

mNQO1 rev 5'-AGGCGTCCTTCCTTATATGCTA-3'

mGCLM for 5'-AGGAGCTTCGGGACTGTATCC-3'

mGCLM rev 5'-GGGACATGGTGCATTCCAAAA-3'

mTNFalpha for 5'-CCCTCACACTCAGATCATCTTCT-3'

mTNFalpha rev 3'-GCTACGACGTGGGCTACAG-3'

mMCP-1 for 5'-TTAAAAACCTGGATCGGAACCAA-3'

mMCP-1 rev 5'-GCATTAGCTTCAGATTTACGGGT-3'

Isolation and culturing primary astrocytes and microglia cells

Whole brains were obtained from postnatal 1 to 3 d old wild-type and YAC128 mouse pups on the FVB/N strain background and placed in Hank's Balanced Salt Solution (Invitrogen) on ice. Meninges were removed and the remaining brain tissue was placed into growth medium (DMEM, 10% FBS, 1% L-glutamine, 1% penicillin/streptomycin), and homogenized. Cells from each brain were pelleted, re-suspended in growth medium, transferred into a T150 flask, and cultured

at 37ºC. Growth medium was replaced after 24 h and thereafter every 7 d. After 18 to 21 d in culture, loosely attached microglia were harvested and seeded at 1.4 x 10^5 cells/ml with pre-incubated conditioned media into 96-well tissue culture plates. Adherent astrocytes were plated at 1.4 x 10^5 cells/ml in 10% FBS media for 24 h in 96-well tissue culture plates.

MIND4-17 activity test on cytokine expression in primary human HD and non-disease monocytes
Cells were isolated from whole blood, as previously described (40). In brief, monocytes were sorted via magnetic cell separation columns using anti-CD14 microbeads (Miltenyi Biotec). Monocytes were seeded at 1 x 10^5 cells per well in 96-well tissue culture plates with R10 media (RPMI culture medium supplemented with 10% FCS, 2 mM L-glutamine, 50 U/ml penicillin and 50 mg/ml streptomycin). After resting for 16 h, the culture media was replaced with R10 media containing either vehicle (DMSO) or MIND4-17 at different concentrations (0.3, 1, and 3 μM). After 24 h of compound treatment, media was changed again using R10 containing both MIND4-17 at the same concentration and, to stimulate cytokine production, 10 ng/ml INF-γ (R&D Systems) and 2 mg/ml lipopolysaccharide (LPS, Sigma-Aldrich). Supernatants were collected at 24 h, and stored at -70°C. Supernatants were analyzed using the human pro-inflammatory II (4-plex) MSD assay measuring IL-1β, IL-6, IL-8 and TNFα. Cytokine levels were normalized to total protein concentration in each well. Cells were lysed in 50 mM Tris pH 8, 150 mM NaCl, 0.5% SDS, and 0.5% Triton X-100 and assayed for total protein concentration using a BCA assay (Thermo-Fisher). Cytokine production in vehicle treated controls peaked at a DMSO concentration that was needed to achieve 1μM compound treatment dose, in an apparent MIND4-17 independent DMSO-mediated effect. Despite this unexplained stimulation by this DMSO concentration, inhibitory effects of MIND4-17 on cytokine production in primary human control and HD monocytes were readily detectable.

To test for toxic effects of MIND4-17 on primary human leukocyte cultures, monocytes were

treated with MIND4-17 but not IFN-γ and LPS, mimicking the treatment duration used in the cytokine profiling experiments (**Fig. S5**). Cell death was measured using a LDH assay (CytoTox-Fluor Cytotoxicity Assay, Promega).

Human iPS cell lines and differentiation of neuronal stem cells

iPSCs were maintained on MEF feeders prepared using mitomycin C. Normal growth medium was: Knockout DMEM/F12 (Life Technologies #12660-012) with 20% knockout serum replacement (Life Technologies #10828-028), 1 mM L-glutamine (Life Technologies #35050-061), 1x MEM non-essential amino acids (Life Technologies #11140-050), 100 μM 2-mercaptoethanol and 50 units/mL penicillin/streptomycin (Life Technologies #15070-063). Genomic DNA was prepared using DNeasy Mini Kit (Invitrogen) from $\approx 10^6$ cells pelleted after accutase passage. 25 μL reaction mix included 0.25 μg genomic DNA, 1xGoTaq Buffer (Promega), 1x GoTaq DNA Polymerase (Promega), 200 μM DNTPs, 200 nM forward/reverse primers, 5% DMSO. PCR products were run on a 4% NuSieve 3:1 Agarose gel (Lonza) at 95V for 3 hrs. Primers and PCR amplification protocol of CAG triplet repeats have been used as previously described (98). Genotype was confirmed by PCR amplification of genomic DNA (**Fig. S6A**).

NSCs were established based on a protocol described for mouse ES cells (82). iPSCs were passaged with 1 mg/mL collagenase type I (Life Technologies #17018-029) in DMEM (Life Technologies #11995-073) on to 0.1% gelatin coated plates (Sigma #G1393) with NSC media: Advanced DMEM/F12 (Life Technologies #12634-028) with 2 mM L-glutamine, 50 units/ml penicillin/streptomycin, retinoic acid-free B27 supplement (Life Technologies #12587-010), N2 supplement; supplemented with 100 ng/mL FGF (Invitrogen #PHG0023), 100 ng/mL EGF (Invitrogen #PMG8041), 5 μg/mL heparin(Sigma #H3149), and 1% knockout serum replacement. Over 5-14 days, bipolar cells were observed to stream out of attached colonies. When cells had formed a 60-80% confluent monolayer of bipolar cells, cells were passaged with Accutase

(Sigma, #A6964) for 2-5 min until detached, then centrifuged 3 min, and remaining clumps of cells disrupted with a p1000 pipet tip. Cells were then re-plated as a single cell suspension 1:1 onto 0.1% gelatin coated plastic, in NSC media, without additional knockout serum and with 20 ng/mL FGF, 20 ng/ml EGF, and 5 µg/ml heparin. Cells were maintained in NSC media, without knockout serum and with 20 ng/ml FGF, 20 ng/ml EGF, and 5 µg/ml heparin on 0.1% gelatin coated plastic and passaged with Accutase as previously described 1:2-1:4 for the first four following passages, then 1:2-1:10 during later passages. NSCs were routinely tested for expression of the radial glial marker nestin by immunofluorescence, and by immunoblotting for presence of neuronal marker β-III-tubulin, absence of astrocytic marker glial fibrillary acid protein (GFAP), and for expression of normal and mutant huntingtin using anti-huntingtin antibody Ab1 (against aa 1-17) by Western blot (**Fig. S6B, C**).

Figure Legends

Fig. S1. MIND4 pharmacokinetics in serum (filled circles) were examined by HPLC analysis in wild-type male C57BL/6 mice (n=3) at 0.5, 1.0, 2, 4, 8, and 24 h at compound treatment dose 50 mg/kg; blood C_{max}=477 ng/ml at 0.5 h time point. Brain levels (red triangle) were analyzed in cortices from mice (n=3) sacrificed at 0.5 h post i.p. injection; C_{brain}=120 ng/ml and respective brain/serum ratio 0.25.

Fig. S2. Characterization of MIND4-17 and its structural analogs. **A)** Structures of MIND4-17 and lead-series of structural analogs. Established NQO1 CD and SIRT2 IC_{50} are shown. **B, C)** Dose-response activity tests of MIND4-17 and MIND4-17 analogs in wild type mouse embryonic fibroblasts (MEF): (**B**) wild type and (**C**) KEAP1-null. Cells were treated with compounds for 24 h. Levels of induced NQO1 protein and β-actin (loading control) were detected by immunoblotting. **D-F)** Testing NRF2 inducing properties of MIND4-17 analogs in structure-

activity relationship (SAR) study of MIND4-17 in ST14A cells. **D**) Structures of MIND4-17analogs: 2872, 2286, 2291, 2907, 2909, used in SAR study. **E, F**) Dose-response activity tests of MIND4-17 analogs in rat embryonic ST14A cells. Levels of NQO1, GCLM and loading control α-tubulin were detected by immunoblotting. Cells were treated with compounds for 24 h. **G, H**) Negative effects of GSH on the NQO1 inducer activity of (**G**) MIND4-17 and MIND4 and (**H**) MIND4-17-33 and MIND4-17-56 (**G**) analogs in Hepa1c1c7 cells. Each compound was incubated in cell culture medium in the presence or absence of 1mM GSH at 37ºC for 30 min before administering to cells. After a 48 h exposure, the NQO1 enzyme activity was determined in cell lysates. Results are shown as average values of 8 replicate wells. The standard deviation in each case was less than 5%.

Fig. S3. Design and synthesis schemes of MIND4-17 analogs 2872, 2286, 2291, 2907, and 2909 for SAR study. **Scheme 1:** a) K_2CO_3, DMF, 100ºC, 1h; b) SnCl2.2H2O, EtOH, reflux; c) $Pd_2(dba)_3$, Xanthphos, Hunig's base, Dioxane reflux. **Scheme 2:** a) EtOH, reflux; b) DCM, Et_3N, rt; c) PCl_3, 1,2-dichlorobenzene, 190ºC. **Scheme 3:** a) Acetone, K_2CO_3 reflux; b) EtOH, reflux; c) 2N KOH reflux; d) K_2CO_3, DMF, 100ºC.

Fig. S4. Treatment with MIND4-17 reduces expression of pro-inflammatory cytokines. **A-F**) Evaluation of NRF2-specific transcriptional responses in rested and LPS-activated iBMM macrophages treated with MIND4-17. Concentration-dependent effects of MIND4-17 on mRNA expression of NRF2-responsive genes *GCLM* (**A**) and *NQO1* (**B**), and inflammatory factors *Il-6* (**C**), *IL-1β* (**D**), *TNFα* (**E**), and *MCP-1* (**F**), and effects of MIND4 at 3 μM on *TNFα* (**G**), Transcriptional expression was measured using qRT-PCR with gene-specific primers and assessed in duplicates (n=2). Means (filled bars) and standard error bars are shown. **H-K**) MIND4 treatment represses expression of inflammatory TNFα protein in brain of HD mouse model R6/2.
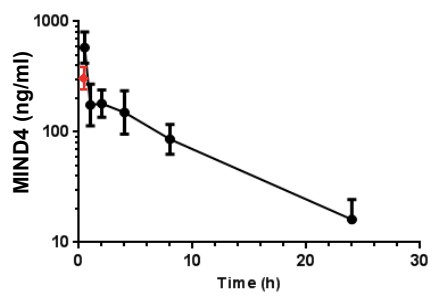
H, I) TNFα and GAPDH protein levels were detected by immunoblotting in cortical extracts from 10-week old wild type (n=7) and R6/2 (n=7) mice (**H**) and in R6/2 mice treated by for 2 weeks with vehicle (control) (n=5) or MIND4 (n=9) at 50 mg/kg, administered by daily i.p. injections (**I**). GAPDH levels were used as loading control. **J**) Quantification analysis of TNFα levels (**H**) in wild type (open bars) and in R6/2 (black bars) brain samples shows no statistical difference. GAPDH protein was used to normalize TNFα levels. **K**) Quantification analysis of TNFα levels (**KI** in vehicle-treated (black bars) and in MIND4-treated (grey bars) R6/2 brain samples. GAPDH protein was used to normalize TNFα levels. MIND4 treatment resulted in statistically significant reduction of TNFα levels in HD cortices. Student's *t*-test, *** P<0.001.

Fig. S5. MIND4-17 mediates anti-inflammatory NRF2 activation responses in human primary monocytes from HD patients and healthy controls. **A-B)** MIND4-17 represses expression of induced inflammatory cytokines in primary monocytes from HD patients and non-disease controls. Expression levels are shown IL-1 (**D**), IL-6 (**E**), IL-8 (**F**), and TNFα (**G**) production by IFN-γ− and LPS-stimulated HD patient monocytes. Cytokine expression, measured by multiplexed ELISAs, was compared in cells treated with 3 μM MIND4-17 or vehicle (DMSO). (Linear mixed model on log transformed data, n=10 non-disease, n=13 for HD patients, *p< 0.05; **p< 0.01, ***p< 0.001.) **E**) MIND4-17 is not toxic for human monocytes. Lack of apparent toxicity of MIND4-17 treatment at tested doses. 48 h treatment of primary human monocytes with MIND4-17 and vehicle does not show any effect on cell viability measured with LDH-assays.

Fig. S6. Characterization of human neuronal HD and non-disease cells, neural stem cells and mature neurons. **A)** PCR analysis of CAG triplet repeat length on genomic DNA from human NSC WT54 (17CAG); HDc116 (containing corrected to wild type 21CAG); HD48 (mutant allele

with 42 CAGs); HD51 (mutant allele with 50 CAGs); HD4-parent of HDc116 (containing 72CAGs). The expected sizes of mutant 42 CAG, 50 CAG and 72CAG PCR products in respective ranges of 180-210 bp, 250-300 bp, and 350-450bp respectively are shown with reference to DNA ladder standard. **B**) Western blot analysis of expression wild type and mutant HTT (indicated by arrows) of NSC cell lines detected using anti-HTT antibody Ab1 against 1-17aa of HTT. **C**) Immunofluorescence microscopy using anti-Nestin antibody of human NSCs derived from iPSCs. Percentages of cells positive for Nestin staining: WT54, 98.75% (n=80 cells); HDc116, 99% (n=301 cells); HD48, 98.92% (n=556 cells); HD51, 98.25% (n=228 cells); HD4, 100% (159 cells).

SI Dataset. (Submitted as Excel spreadsheet table). Quantitative mass-spectrometry data for reactive cysteines modified by MIND4-17 treatment. Cysteine reactivity in proteomes pre-treated with MIND4-17 (Heavy-labeled) were compared to DMSO-treated samples (Light-labeled). For every cysteine-containing peptide, a heavy:light ratio was calculated that reflects the extent of cysteine reactivity in the inhibitor-treated versus DMSO samples. A ratio of 1 indicates that there was no change in cysteine reactivity, whereas ratio values >>1 show a loss in cysteine reactivity upon inhibitor treatment. Four cysteine-containing peptides with ratio >2, modified by MIND4-17, are shown at top of the table and highlighted in green.

A
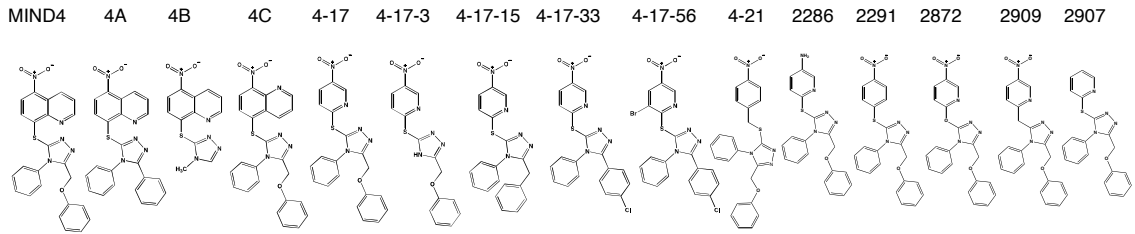
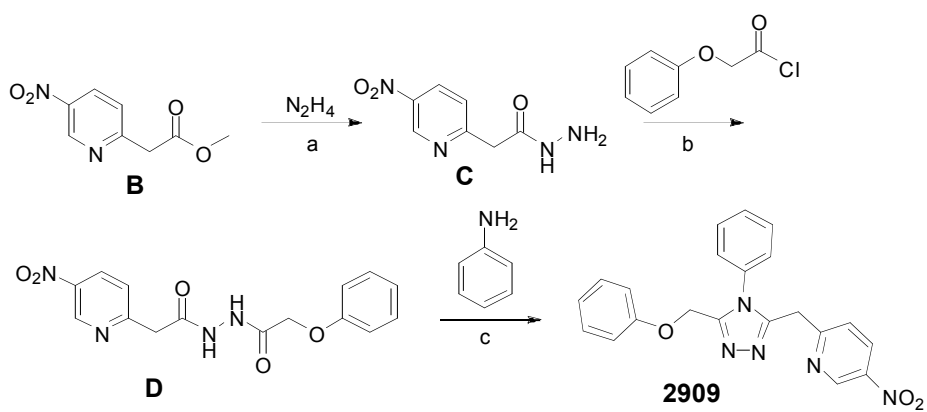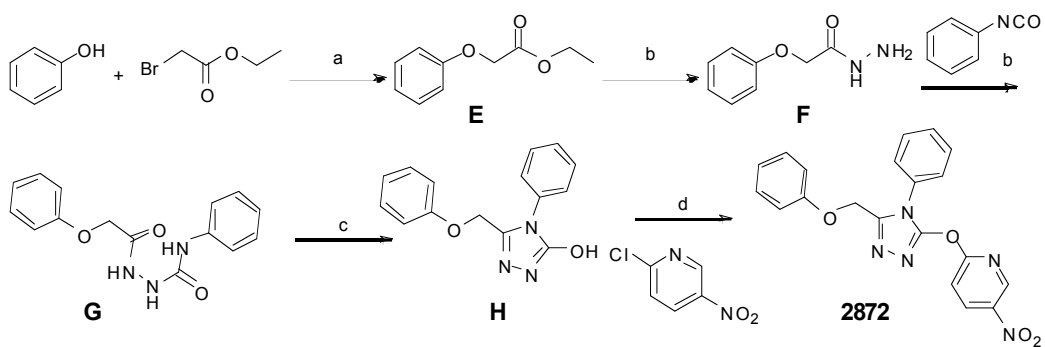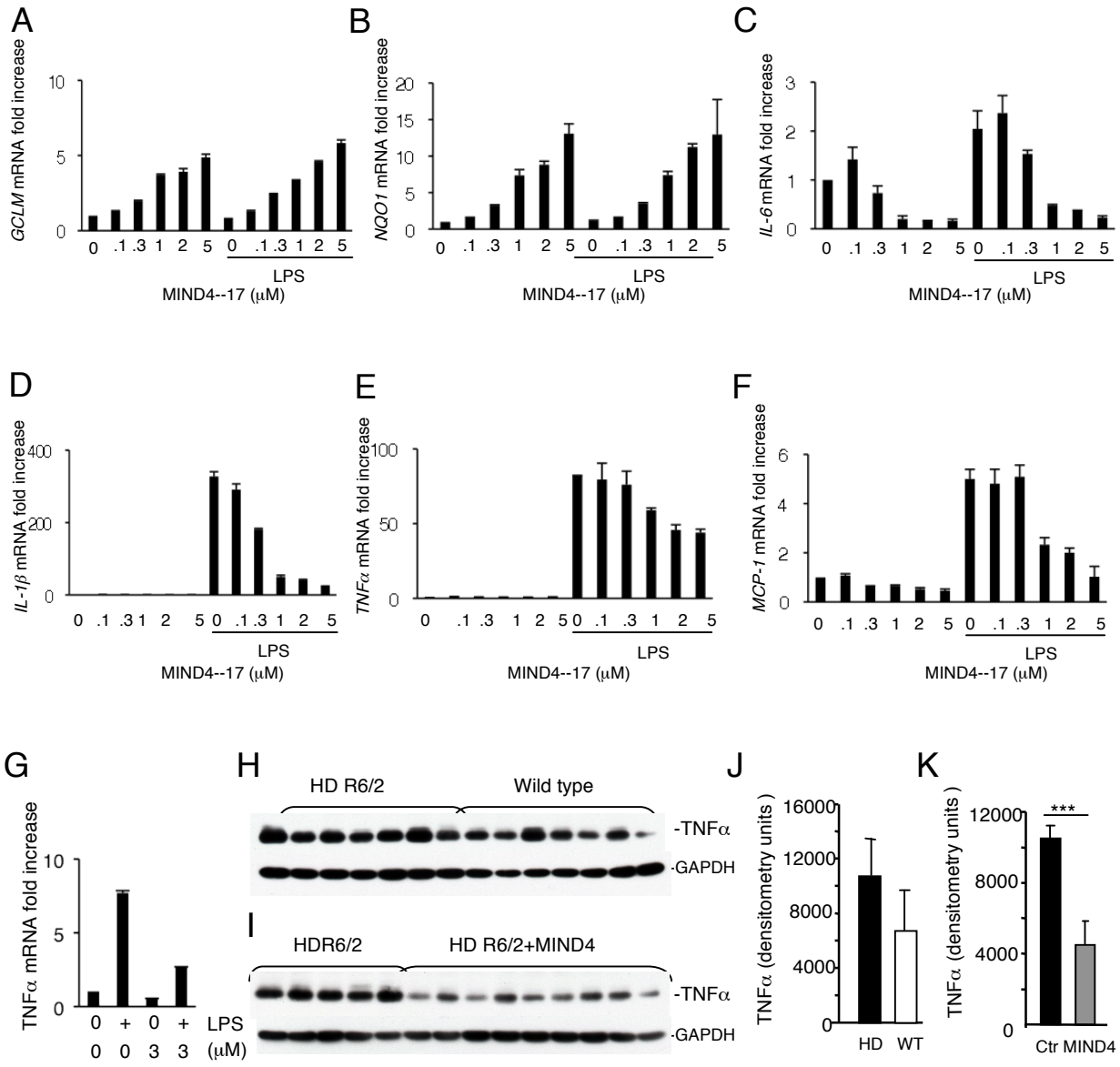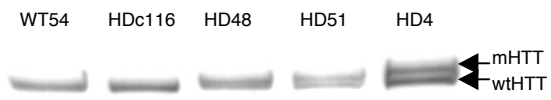|	MIND4	4A	4B	4C	4-17	4-17-3	4-17-15	4-17-33	4-17-56	4-21	2286	2291	2872	2909	2907
SIRT2 IC$_{50}$ (μM)	3.5	7.5	>50	>20	>50	>50	>50	7.5	0.75	10	n/d	n/d	n/d	n/d	n/d
NQO1 CD (μM)	1.3	1	2	5	0.15	7.5	0.3	0.3	2.5	>10	2.5	10	n/d	n/d	n/d
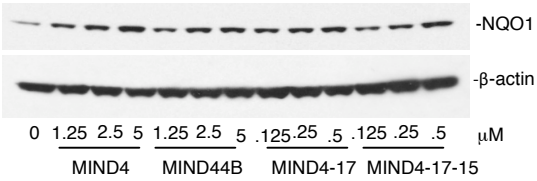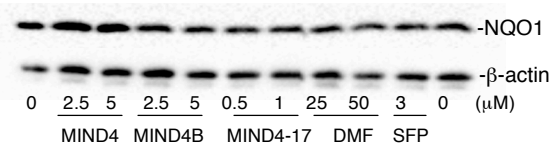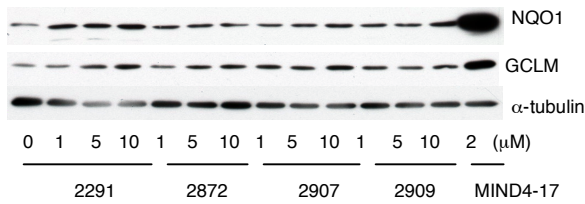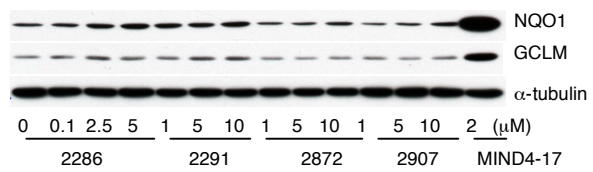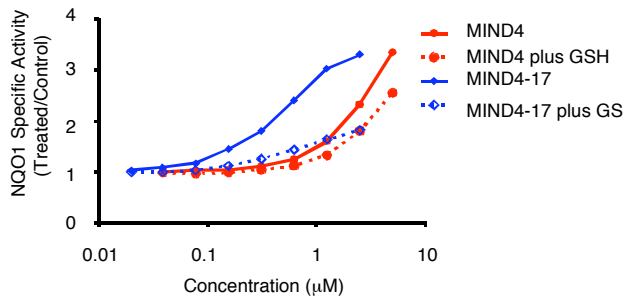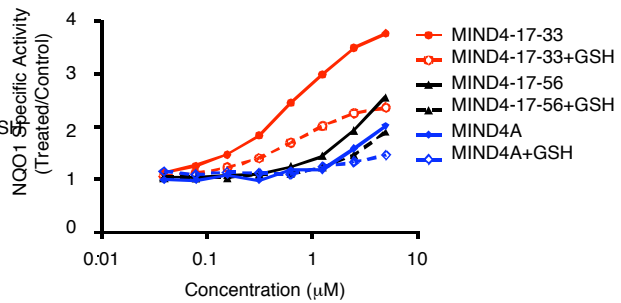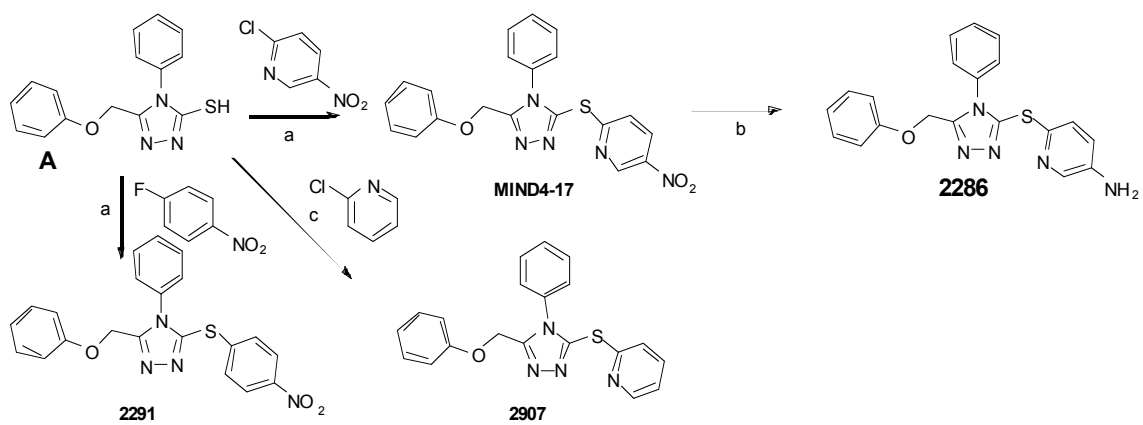
Scheme 1

Scheme 2

Scheme 3

A

B

C

D

E

A

DNA ladder · WT54 · HDc116 · HD48 · HD51 · HD4

400bp-
300bp-
200bp-
100bp-

B

WT54 · HDc116 · HD48 · HD51 · HD4

← mHTT
← wtHTT

C

WT54 · HDc116 · HD48 · HD51 · HD4